AC
.H3
no.F86

ms

Acoustic bottom loss computation: a graz
AC .H3 no.F86 15292
Fisher, Craig A.
SOEST Library

MAR 11 1987

ACOUSTIC BOTTOM LOSS COMPUTATION:

A GRAZING ANGLE MATCHING METHOD

APPLIED TO DEEP OCEAN BOREHOLE DATA

A THESIS SUBMITTED TO THE GRADUATE DIVISION OF THE
UNIVERSITY OF HAWAII IN PARTIAL FULFILLMENT
OF THE REQUIREMENTS FOR THE DEGREE OF

MASTER OF SCIENCE

IN GEOLOGY AND GEOPHYSICS

DECEMBER 1986

By

CRAIG ALAN FISHER

HAWAII INSTITUTE OF GEOPHYSICS
LIBRARY

Thesis Committee:

Frederick K. Duennebier
L. Neil Frazer
Gerard J. Fryer

We certify that we have read this thesis and that in our opinion it is satisfactory in scope and quality as a thesis for the degree of Master of Science in Geology and Geophysics.

THESIS COMMITTEE

Chairman

ACKNOWLEDGEMENTS

This work would not have been completed without the help of many people. Neil Frazer brought the data set to my attention. Fred Duennebier gave me ready access to the data and encouraged me as the work proceeded. Chip McCreery took time to help me understand how to obtain absolute levels of particle motion from raw data. I have benefitted from discussions with Paul Anderson, Bob Cessaro, Dan Miller, David Novelo, Mrinal Sen and other fellow students. My family and friends have been supportive and understanding during my involvement with this study. My thanks go to all these individuals. Finally, I am grateful to the Office of Naval Research for funding this work.

ABSTRACT

Ocean bottom reflection loss (BRL) cannot be computed by traditional methods from data recorded in a borehole. A grazing angle-dependent loss, called bottom transmission loss (BTL), is incurred by a ray passing through the overlying sediments and basalts. BTL must be removed before BRL can be computed. A new BRL computation method implicitly removes this extraneous angle-dependent loss. The new technique, called the grazing angle matching empirical method (GAME), is more general than other methods of computing BRL. GAME uses multiple bottom-interacting rays with the same grazing angle to obtain BRL estimates. GAME is "self-calibrating" in grazing angle as well as in frequency, allowing the source and receiver directionality to vary in the vertical-radial plane. BRL estimates computed by GAME from borehole data are consistent. These results closely match those of Chapman (1983) and Focke, et al. (1980), computed by another method from other deep ocean data sets. BTL was also computed from the borehole data, yielding consistent results. BTL is greater (by 5 to 10 dB) for particle motion in the transverse horizontal direction than for particle motion in the radial-vertical plane. BRL results are the same for both particle motions.

TABLE OF CONTENTS

ACKNOWLEDGMENTS iii

ABSTRACT iv

LIST OF TABLES vii

LIST OF ILLUSTRATIONS viii

LIST OF ABBREVIATIONS x

1. INTRODUCTION 1

2. THEORY 8

   2.1 General 8

   2.2 A new technique: GAME, the grazing angle matching empirical method of approximating the incident ray energy-flux density 9

   2.3 Comparison of GAME with the semi-empirical (or S-E) approximation to incident ray energy-flux density 13

   2.4 Comparison of GAME with the direct arrival empirical (or DAE) approximation to incident ray energy-flux density ... 16

3. DATA 20

   3.1 Experiment 20

   3.2 Environment 21

   3.3 Raw Data 28

4. A GAME ALGORITHM 32

5. RESULTS AND DISCUSSION 35

   5.1 Characteristics of the arrivals 35

5.2 Propagation loss 42

5.3 Bottom reflection loss 50

5.4 Bottom transmission loss 55

6. SUMMARY 60

REFERENCES 61

APPENDIX A Energy-Flux Density Computation 66

APPENDIX B Data Reduction Outline 70

LIST OF TABLES

Table		Page
I	Physical properties model of seawater, sediments and basalts .	25
II	Transfer functions	38

LIST OF ILLUSTRATIONS

Figure		Page
1.1	The geographic location of the experiment	5
1.2	The family of eigenrays studied here	7
3.1	Bathymetry in the study area	22
3.2	Spectrogram of the data recorded during the experiment	24
3.3	Representative single channel reflection section in the area	27
3.4	Time domain record section of the data set	29
3.5	The four bottom-interacting eigenray families for a water column receiver	31
5.1	Water wave and noise particle velocity spectrum levels	37
	a.) Using PSV particle motions	
	b.) Using SH particle motions	
5.2	Head wave and noise particle velocity spectrum levels	41
	a.) Using PSV particle motions	
	b.) Using SH particle motions	
5.3	Water wave propagation loss versus range	45
	a.) Using PSV particle motions	
	b.) Using SH particle motions	
5.4	Water wave propagation loss versus grazing angle	47
	a.) Using PSV particle motions	
	b.) Using SH particle motions	
5.5	Smoothed and corrected water wave propagation loss	49
	a.) Using PSV particle motions	
	b.) Using SH particle motions	

5.6 Bottom reflection loss (BRL) estimates 52

a.) Using PSV particle motions

b.) Using SH particle motions

5.7 Theoretical plane-wave reflection coefficients for an incident P-wave at the water/sediment and sediment/basalt interfaces .. 54

5.8 Comparison of BRL results from this study with results from two other studies 56

5.9 Bottom transmission loss (BTL) estimates 58

a.) Using PSV particle motions

b.) Using SH particle motions

LIST OF ABBREVIATIONS

a	A subscript suffix, meaning "assumed".
A	Azimuth.
BTL	Bottom Transmission Loss
BRL	Bottom Reflection Loss
c	Velocity of the medium at the receiver.
dA	Correction to azimuth.
DAE	Direct arrival empirical method of computing BRL.
DN	Difference between number of bottom interactions of the two arrivals used in the BRL ratio (2.1).
e	Error term in BRL and BTL equations (Appendices B.13 and B.14).
E	Energy-flux density, used to compute intensity from broadband data.
f	Frequency.
Δf	Frequency band.
F	Instrument transfer function.
FR	A weighting function subscript, denoting "frequency" weights.
GAME	Grazing angle-matching empirical method of computing BRL.
i	The square root of -1.
I	Intensity.
j	Discrete time index.
Δj	Discrete frequency band.
j1	Frequency index for the lowest frequency in a band.
j2	Frequency index for the highest frequency in a band.

J1 Arrival index for the lowest order arrival in a window (2.8).

J2 Arrival index for the highest order arrival in a window (2.8).

k Discrete frequency index.

K Spreading exponent.

L Travel path length of a ray, computed by ray tracing.

m A subscript, standing for "assumed".

M The order of the reference ray at a given grazing angle.

MSPV Mean-square particle velocity.

n The number of data samples.

nf The number of discrete frequencies averaged over (4.1).

nJ The number of BRL estimates averaged over (4.2).

nr The number of ranges averaged over (4.1).

N The order of a reflected eigenray.

p Pressure.

PDC Practice depth charge.

PL Propagation loss.

PSV Particle motion in the radial-vertical plane.

PV A subscript meaning particle velocity.

r Shot offset, or range, measured horizontally.

ρ Density.

R A weighting function subscript, denoting "range".

RMS Root Mean Square, defined as the square root of the sum of squared elements divided by the number of elements.

s Ocean bottom slope.

S A subscript denoting "source".

S-E	Semi-empirical method of computing BRL.
SDL	Surface decoupling loss.
SH	Particle motion in the transverse horizontal direction.
Spr	Spreading Loss
SN	A weighting function subscript, denoting "signal-to-noise" ratio.
SUM	The sum of the weights in a weighted average computation.
SUS	Source of Underwater Sound.
t	Time.
u	Particle velocity.
W	A weighting function, its subscript defines which one it is.
x	The data in the time domain.
X	The data in the frequency domain.

1. INTRODUCTION

Bottom reflection loss (BRL) is a measure of energy lost when an acoustic wave in the ocean interacts with the ocean bottom. BRL is a function of the grazing angle and frequency of the acoustic wave, as well as the physical properties of the ocean bottom. BRL results obtained in explosive source experiments may also depend on the data window length. This is because head waves, reflections from deep interfaces, and interbed multiples may be received outside the data time window. (These "non-specular" arrivals may also interfere with the specular reflection, complicating the analysis of BRL.) BRL measurements are made for two reasons: 1.) to better understand the effect of bottom interactions on sound propagation in the ocean and 2.) to determine ocean bottom structure.

Several mechanisms of ocean bottom reflection loss have been identified, including scattering, shear conversion and head wave generation at interfaces, and intrinsic attenuation in the sediments and in the subbottom. Assessment of these effects has been the subject of a large number of theoretical modeling papers (e.g. Fryer, 1978; Hawker & Foreman, 1978; Rutherford & Hawker, 1978; Hawker, 1979; Hawker et al., 1979; Rutherford et al., 1979; White, 1979; Vidmar, 1980a,b,c; White & Stephen, 1980; Stoll & Kan, 1981; Daniels & Vidmar, 1982; Oakley & Vidmar, 1983; Hampton, 1985; Stern et al., 1985).

Among the methods that have been used to determine ocean bottom structure from BRL results are parametric inversion and forward

modeling. Mitchell & Focke (1979) inverted the bottom reflection loss of rays refracted upward from the sediment column at low grazing angles and estimated a sedimentary compressional wave attenuation profile. Forward modeling of measured BRL has been used to evaluate theoretical ocean bottom velocity structures by DiNapoli et al. (1980), and to estimate the compressional wave velocity gradient and attenuation constant in ocean bottom sediment by Spofford (1980).

Urick (1983) defined BRL in terms of the ratio of reflected to incident intensity of a bottom interaction. BRL is intrinsically a plane wave function and can therefore be understood in terms of the slant stack (or tau-p) transformation well known in seismology. A slant stack converts spherical-wave data from the experimental domain of time and distance into the plane-wave domain of ray parameter and delay time (or, equivalently, into the domain of grazing angle and delay time). The BRL function can be defined as the normalized integrated power, at each grazing angle and frequency, of the slant stack transformation of a single well-defined reflected arrival from the ocean bottom. Under this definition BRL is computed as follows: 1.) The raw data are windowed so only bottom reflected arrivals from a single family are non-zero (the bottom reflected arrivals are classified into families in Section 3.3), 2.) The data are slant stacked, then squared and integrated over delay time at each grazing angle and frequency, 3.) The integrated power is normalized by the power incident at each grazing angle and frequency, and corrected for spreading differences. A similar result, power integrated over delay time at each ray parameter using slant-stacked

finite record-length data, has been proposed by Brocher & Phinney (1981) as a constraint on velocity-depth structure inversion of the delay-time function of a slant stack.

Because BRL is intrinsically a plane-wave function, it is difficult to measure. The most reliable measurements of BRL are probably obtained by performing a seismic experiment to measure bottom structure, then performing forward modeling to predict BRL. Such parametric estimates of BRL are not always practical, either because of expense or the difficulty of measuring bottom structure. Non-parametric or direct measurements of BRL attempt to obtain the function directly from the ratio of reflected to incident energy. Direct methods of BRL computation differ in the way the intensity of the reference ray, used to approximate the incident ray intensity, is obtained. Three methods have been reported in the literature: 1.) The direct source-to-receiver ray has been used as the reference ray (e.g. Bucker et al., 1965; Hastrup, 1969,1980; Santaniello et al., 1979). Method one is called the direct arrival empirical method (DAE) in this thesis. 2.) A semi-empirical incident ray intensity based on a known source level has also been used (Mitchell et al., 1980; Chapman, 1980,1983). Method two is termed the semi-empirical method (S-E) in this thesis. 3.) A Backus-Gilbert linear inversion technique has been proposed as a means of implicitly computing the complex reflection coefficient of the ocean bottom (Schoenberg, 1978). Method three is not discussed further in this thesis.

In the current study a new direct method is proposed. This

method approximates the incident ray intensity in a new way. The intensity of a ray with the same grazing angle as a reflected ray, but with fewer bottom interactions, is used to approximate the incident intensity of the reflected ray. Specular reflection from the ocean bottom is assumed when computing grazing angles. The new method is called the grazing angle matching empirical method (GAME). GAME can be used to deduce bottom reflection loss from data obtained with water column, ocean floor, or borehole receivers; whereas the other methods can only be applied in a limited fashion to reduce borehole data. DAE cannot be used on borehole data unless the direct and reflected arrivals in the ratio have the same grazing angle. S-E cannot deal with borehole data unless the water-to-receiver bottom transmission loss as a function of grazing angle is known in advance.

GAME is similar to the direct arrival approximation technique, but in the new technique the direct ray has the same grazing angle as the reflected ray. The new procedure (GAME) goes one step further, in that if a direct ray is not available, a reflected ray with the same grazing angle (but fewer reflections) can be used as the reference ray. Because it matches grazing angles of reflected and reference rays, the "self-calibrating" property of the direct arrival technique is extended here to include the directionality of the source and receiver (discussed in Section 2.3).

In this paper GAME is applied to a data set recorded in DSDP Hole 581C located in the NW Pacific Basin 1100 km east of Hokkaido and 750 km south of the Kamchatka peninsula (Figure 1.1). The data

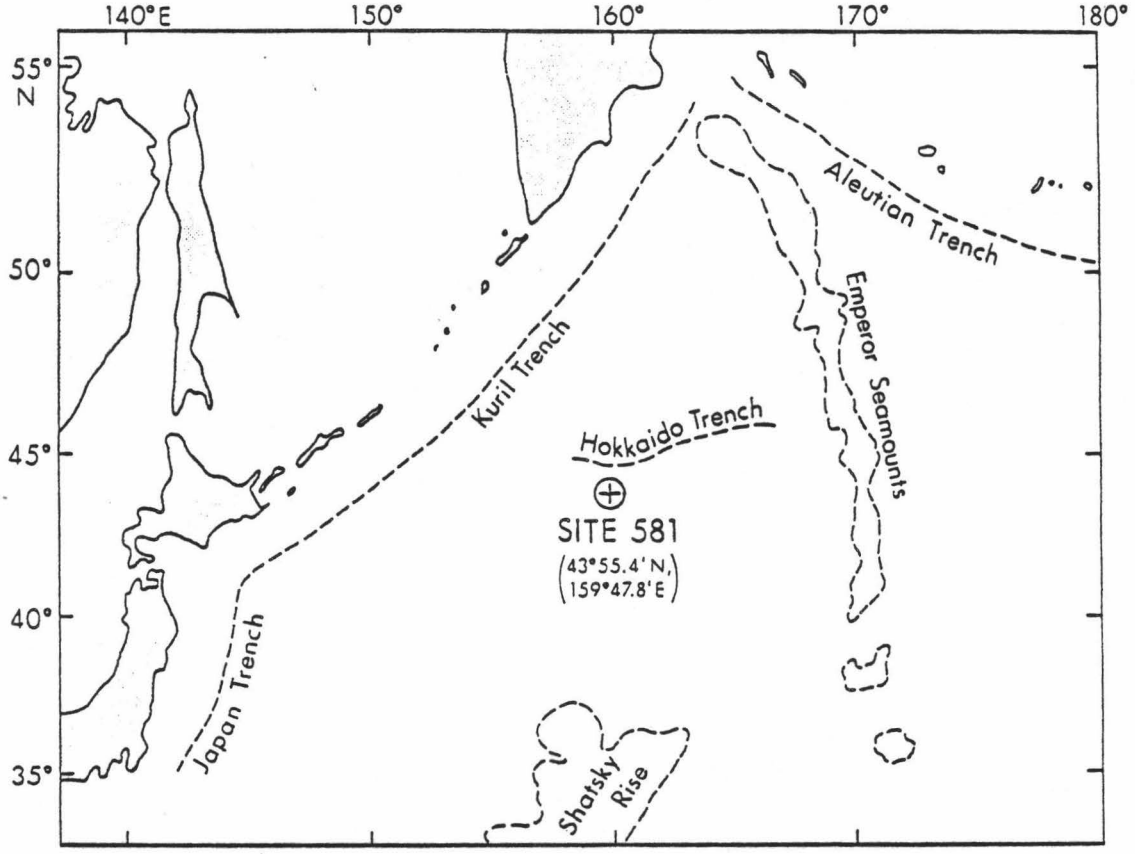

Figure 1.1 The site of the borehole in the NW Pacific Ocean. (From Duennebier, et al., 1986a.)

collection is discussed by Duennebier et al. (1986a), who used a three-component borehole seismometer package (Byrne et al., 1986). SUS (sources of underwater sound) charges were dropped along a line out to 90 km from the receiver to generate the arrivals studied here.

It is necessary to define some terms. Geometric rays carrying a portion of the total acoustic field are sometimes called "eigenrays" (Urick, 1983). In ocean acoustics, These arrivals are sometimes termed "water waves" to distinguish them from "ground waves" (Pekeris, 1948). The latter spend a portion of their travel path as body waves in the ocean bottom. Ray "order" is an integer quantity specifying the order in which bottom-interacting eigenrays are received near the source (e.g. Chapman, 1980). Since the data in this study were recorded in a borehole, the eigenray order equals the number of bottom interactions of the eigenray. In general an eigenray of order N has N-1 bottom reflections, plus one transmission through the bottom to the receiver, for a total of N bottom interactions. For example, the first order eigenray arrives directly from the source. It interacts with the bottom once, being transmitted through the water/sediment and sediment/basalt interfaces down to the receiver. The second order eigenray from the same source interacts with the bottom twice: It has one bottom bounce, plus transmission through the interfaces to the receiver. All the eigenrays used here are shown schematically in Figure 1.2 and compared with the general case in Section 3.3.

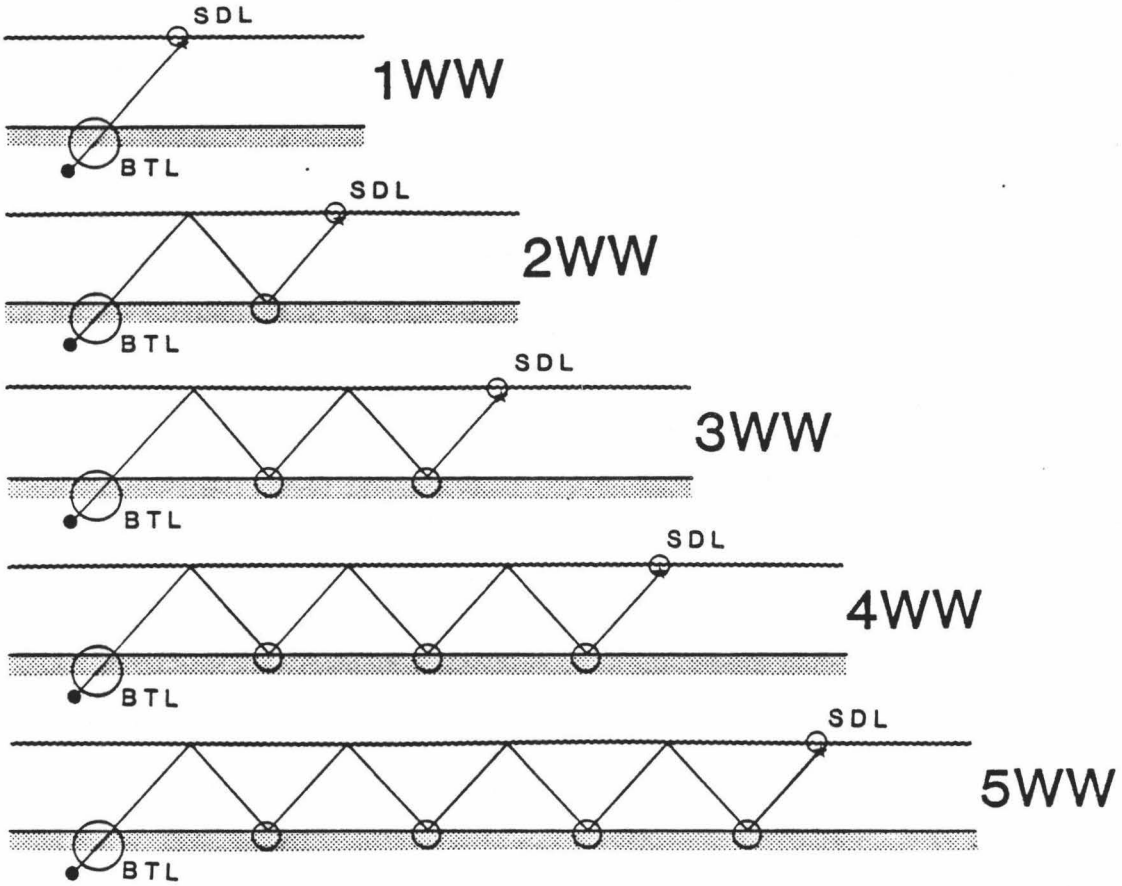

Figure 1.2 The eigenrays used in this study. The notation (NWW) indicates the number of bottom interactions (N) of the ray. Locations of bottom reflection loss (BRL), bottom transmission loss (BTL), and surface decoupling loss (SDL) are circled.

2. THEORY

2.1 General.

For the simple case of a single ray reflected once from the ocean bottom, bottom reflection loss (BRL) is defined as the ratio of the reflected ray intensity to the intensity of the incident ray at the ocean bottom (expressed in dB) so that

$$\text{BRL} = -10\log_{10}[\text{ Reflected ray intensity / Incident ray intensity }]$$

(Urick, 1983). The incident ray intensity, however, is not easily obtained, and is usually estimated. The term "reference ray" intensity is used here to refer to the incident ray intensity estimate. BRL can be expressed in terms of the reference ray as

$$\text{BRL} = -10\log_{10}[\text{ Reflected ray intensity / Reference ray intensity }] / \text{DN}, \qquad (2.1)$$

where DN is the difference in number of bottom bounces between the reflected and reference rays. In (2.1) the intensities of both rays are assumed to be measured at the point of reflection on the ocean bottom. The same result will be obtained, however, as long as both intensities are measured at (or referenced to) the same location in the water column, provided this does not introduce additional attenuation or

caustic formation.

When an impulsive source is used, ocean acoustics problems are studied in terms of "energy-flux density", defined as instantaneous intensity integrated over the time period containing the signal (Urick, 1983). In the following theoretical discussions energy-flux density is used. An expression for this quantity is derived in Appendix A.

Calibrated quantities, such as the receiver response, are given as spectrum levels in ocean acoustics. "Spectrum level" means that a one Hertz bandwidth is assumed (Urick, 1983, p. 14). Thus, a quantity such as RMS particle velocity is expressed in units of RMS particle velocity per Hertz or as RMS particle velocity spectrum level.

2.2 A new technique: GAME, the grazing angle matching empirical method of approximating the incident ray energy-flux density.

I introduce here a new BRL computation method called GAME, or the "grazing angle matching empirical" method, after the way the energy-flux density of the reference ray is computed. GAME employs an eigenray of order M (where $M > 0$), at grazing angle g, to approximate the incident ray energy-flux density for reflected eigenrays of order N (where $N > M$) at the same grazing angle. This new technique is designed to analyze data from a borehole receiver (but handles all cases). Hydrophone or vertical geophone data can be used, as well as the radial or transverse component of orthogonal horizontal geophones, or some vector combination of these.

For the eigenray (i.e. water wave) of order N at frequency f and grazing angle g, we obtain

$$BRL(f,g,N) = -10\log_{10}\{ [E_m(f,g,N) / Spr_a(N,g)] / [E_m(f,g,M) / Spr_a(M,g)] \} / [N - M(f,g)], \quad (2.2)$$

where M is the order of the reference eigenray. The terms E_m are the two measured energy-flux densities. The terms Spr_a are geometric spreading losses. At each frequency and grazing angle BRL estimates can be calculated for all N, where N > M. An average of these estimates yields the final BRL value for each frequency and grazing angle; the details of this operation will be described in Chapter 4.

Spreading losses are ratios of the energy-flux density expected in a ray at the receiver location to the energy-flux density expected at some standard distance from the source, assuming lossless media. (Appendix B.5 discusses the spreading loss assumption used in applying GAME to borehole data in this thesis.)

The measured, noise-corrected energy-flux densities of the eigenrays are denoted E_m. $E_m(M)$ and $E_m(N)$ in (2.2) correspond to the reference and reflected eigenrays, respectively. These energy-flux densities, computed from broadband data (using Equation A.11), are

$$E_m(f,g,J) = (\rho c)(t_n - t_1) [|X_m(f,g,J)|^2 / F_{MSPV}(f,g)]. \quad (2.3)$$

Here ρ is the density of the earth material at the receiver location.

The quantity $X_m(f)$ is the measured geophone response, and F_{MSPV} is the receiver transfer function for mean-square particle velocity (converting the raw geophone response to mean-square particle velocity).

An important property of GAME is that the technique does not require that the receiver transfer function be known. In the GAME formulation, when (2.3) is substituted into (2.2) the receiver response cancels. In addition the impedance of the medium and the data window length (assumed to be constant) cancel. Only the raw geophone responses are required.

For the purpose of BRL computation GAME defines the measured energy-flux densities to be

$$E_m(f,g,J) \equiv [E_S(f,g)-SDL(f,g)-Spr(J,g)] - [J-1]BRL(f,g) - BTL(f,g). \qquad (2.4)$$

Where E_S is the energy-flux density at a standard distance from the source (relative to unit energy-flux density). Spr is the loss due to geometrical spreading (relative to no loss of energy-flux density at a standard distance from the source). BTL is the ocean bottom transmission loss and SDL is the surface decoupling loss (both relative to no loss of energy-flux density). Formal definitions of BTL and SDL will be given later. The locations along the raypaths where BRL, BTL and SDL occur are circled in Figure 1.2 (locations of BTL and SDL are also labeled).

The losses BTL and SDL are implicitly removed by GAME. They

are functions of both grazing angle and frequency, and are incurred once in both the reference and reflected eigenrays. These losses implicitly cancel in the energy-flux density ratio (2.2) because the eigenrays used in the ratio have the same grazing angle and frequency.

The quantity BTL is the loss incurred during the one-way traverse through the ocean bottom (including both the water/sediment and sediment/basalt interfaces) to the borehole receiver. BTL contains losses due to scattering, head wave generation, and shear conversion at interfaces, scattering and intrinsic attenuation in the subbottom, and, in the basalt, evanescent decay of both compressional and converted shear waves. For a receiver located in the water column or on the ocean bottom, BTL = 0.

SDL results from interference between upgoing and downgoing rays when a source or receiver is near an interface. In the case of a near-surface source with a borehole receiver the effect is due to interference of an initially upgoing ray, reflected downward by the sea surface, with an initially downgoing ray (these rays are shown in Figure 3.5d and 3.5b, respectively). This interference is sometimes called image-interference or the Lloyd's mirror effect. Explicit corrections for the effect of SDL on bottom reflection loss measurements have been given by Bannister & Pedersen (1981).

GAME also limits the critical angle effect often called "negative bottom loss", associated with interference from emerging head waves (Stickler, 1977; Santaniello, et al., 1979). Such effects will not appear in the results of GAME. As both incident and reference rays

have identical bottom interactions, the head wave interference cancels exactly. Other interference effects, due to such phenomena as sediment reverberations and caustic formation, can be limited by using a narrow data window.

Errors in the quantities and assumptions of (2.2) are assumed to be small. Such errors may be systematic, for example due to attenuation in the water column (Focke et al., 1982), or random, due to such things as inhomogeneous bottom roughness (Tuteur, 1976). Since errors are assumed to be small, the combination of many such discrepancies has a Gaussian distribution centering on zero error. The effect of these errors is further reduced when several BRL estimates are averaged (this point is elaborated on in Appendix B.15).

2.3 Comparison of GAME with the semi-empirical (or S-E) approximation to incident ray energy-flux density.

One method of computing BRL involves reconstructing the incident energy-flux density based on theoretical, or semi-empirical, information (e.g., Mitchell, et al., 1980; Chapman, 1980,1983). I will call this method "S-E". Implementing S-E requires use of a well known source (such as "S.U.S." practice depth charges), a calibrated receiver and accurate ray tracing. BRL computed by S-E is

$$BRL(f,g,N) = -10\log_{10}\{ E_m(f,g,N) / [E_{S,a}(f)/Spr_a(N)/SDL_a(f,g)] \} / N. \qquad (2.5)$$

Here $[E_{S,a}(f)/Spr(N)/SDL_a(f,g)]$ is the energy-flux density of the reference ray at the receiver location. $E_{S,a}$ (for $E_{S,assumed}$) is a source level calibration (defined as the energy-flux density at a standard distance from the source). SDL_a (for $SDL_{assumed}$) is the assumed surface decoupling loss (i.e. image-interference).

The measured energy-flux densities computed with broadband data are (from Appendix A)

$$E_m(f) = (\rho c)(t_n - t_1) \; [\; |X_m(f)|^2 \; / \; F_{MSPV,a}(f) \;], \tag{2.6}$$

where $F_{MSPV,a}$ (for $F_{MSPV,assumed}$) is a particle velocity calibration curve for the receiver. (Notice that the receiver response is assumed to be independent of grazing angle.) For the purpose of BRL computation S-E defines the measured energy-flux densities this way:

$$E_m(f,g,J) \equiv [E_S(f) - Spr - SDL(f,g)] - [N]BRL(f,g,N). \tag{2.7}$$

The terms in this expression have been defined in reference to (2.4) above. Notice that the source level is assumed to be independent of grazing angle, in contrast to (2.4) in GAME.

One approach of using S-E involves forward modeling the propagation loss of identified rays falling within the data window (Hampton, et al., 1978 and Mitchell, et al., 1980). In this approach the contributions of rays identified as arriving in the window are coherently summed at each frequency. Equation 2.5 then becomes

$$BRL(f,g,\bar{N}) = -10\log_{10}\{ [E_m(f,g,\bar{N}) / E_{S,a}(f)] / \sum_{J=J1}^{J2} [[Spr_a(J)][SDL(f,g,J)]] \} / \bar{N}. \quad (2.8)$$

Here J1 and J2 are the lowest and highest order arrivals in the data window, respectively, and $\bar{N}$ is the mean number of bottom interactions of the arrivals falling in the data window. The sum in (2.8) is called "reference propagation loss", the energy-flux density ratio is called "measured propagation loss" and cylindrical spreading over shot range is assumed.

S-E requires knowledge of source and receiver calibration. However, differences between the calibration and experimentation environments limit the accuracy of S-E (Ballagh, 1982). Unlike S-E, GAME is "self-calibrating" in the experimental environment, which should be advantageous in many situations. (Recall that the receiver response cancels in GAME, and that the source term is not needed.) In addition SDL is corrected implicitly in GAME. Explicit corrections, with with their attendant inaccuracies, are not needed in GAME.

S-E is not applicable to borehole data. Borehole data includes significant losses incurred on the final traverse from the water column to the subbottom receiver (included in the term BTL of Equation 2.3). S-E could be used with borehole data if an explicit correction for BTL(f,g) was applied.

2.4 Comparison of GAME with the direct arrival empirical (or DAE) approximation to incident ray energy-flux density.

Another BRL computation method approximates the incident ray energy-flux density using the measured energy-flux density of the direct source-to-receiver ray. I will call this method "DAE". BRL computed with DAE is

$$BRL(f,g,N) = -10\log_{10} \{ [E_m(f,g,N)/Spr_a(N)] / [E_m(f,g_d,1)/Spr_a(1)] \} / [N-1]. \tag{2.9}$$

Here N is the order of the reflected ray (with N-1 bottom bounces), g is the grazing angle of the reflected ray and g_d is the grazing angle of the direct arrival at the same range as the reflected ray. The order of the direct arrival is one (1). This method has been used by Bucker, et al. (1965), Hastrup (1969), and Santaniello, et al. (1979), for example.

$E_m(f,g_d,1)$ and $E_m(f,g,N)$ are the measured energy-flux densities of the direct arrival and a bottom reflected arrival, respectively. When computed from broadband data (using Equation A.11) these quantities are

$$E_m(f,g,J) = (\rho c)(t_n-t_1) \; [\; |X_m(f,g,J)|^2 / F_{MSPV}(f) \;]. \tag{2.10}$$

Notice that the particle velocity transfer function is assumed to be independent of grazing angle here, in contrast to the corresponding

definition (2.3) used in GAME.

The measured energy-flux densities used in DAE are defined to be

$$E_m(f,g,J) \equiv [E_S(f)-Spr(J)] - [J-1]BRL(f,g) \qquad (2.11)$$

for the purpose of BRL computation. The terms in this expression have been defined in reference to (2.4) above. Notice the source level is assumed to be independent of grazing angle here, in contrast to the corresponding factorization (2.4) in GAME.

DAE has been celebrated as being "self-calibrating" in frequency (Santaniello, et al., 1979). The DAE formulation removes the frequency-dependent receiver response from the problem, since ratios of empirical energy-flux densities are computed at each frequency and this function cancels in these ratios. Additionally, and in contrast to S-E, this formulation removes the frequency-dependent source level from the problem, since ratios of empirical energy-flux densities are computed at each frequency. GAME shares with DAE this property of implicitly handling source level frequency dependence.

However, DAE is not "self calibrating" in grazing angle. (Note that the direct and reflected rays in Equation 2.9 in general have different grazing angles.) This has caused complications in computing BRL--leading to ad hoc solutions. For example, differences in transducer directionality have required explicit corrections to BRL results (Bucker et al., 1965). In another case the data window length applied to reflected arrivals was decreased as the grazing angles of

these rays decreased to correct for the relative "time-compression" of the reflected arrivals (Hastrup, 1969). Such explicit corrections to the data or algorithm are not necessary in GAME (except in unusual circumstances, such as when the receiver or source directionality functions change during the experiment).

GAME is "self-calibrating" in grazing angle, since it involves taking energy-flux density ratios of two rays with the same grazing angle. This property of GAME means that it properly accounts for the directionality of both the source and the receiver in the vertical-radial plane. This quality is indicated in (2.3) and (2.4) by the grazing angle-dependence stipulated for the receiver and source terms, respectively. One result of this property is that a horizontally anisotropic source array could be used in a BRL measurement without empirical corrections (if the source alignment relative to the shot line is kept constant). For example, Aquaflex could be used as a source (White, 1979). Applications of DAE in the literature do not have this property of implicitly removing source directionality.

Bannister and Pedersen (1981) pointed out that if shallow explosive sources are used and low frequencies are studied, surface decoupling loss (SDL) is significant at low grazing angles and should be corrected before computing BRL. Under these conditions SDL should be included in (2.11) and explicit corrections for this loss should be made in (2.9). In contrast, GAME should implicitly handle the dipole directionality of shallow explosive sources at low frequency.

In addition, since BTL (bottom transmission loss, defined and

discussed in Section 2.2) is ignored, DAE cannot handle borehole data. BTL is neither explicitly included, nor implicitly accounted for in DAE.

DAE could be modified so that the direct ray has the same grazing angle as the reflected ray (I will call this method "modified DAE"). Then SDL and BTL will be the same for both rays, and will cancel in the ratio. Source and receiver directionality would also be implicitly removed in this modification. Explicit corrections would be unnecessary. Modified DAE is similar to GAME.

Although similar, modified DAE still differs from GAME. When the direct arrival is not sampled across the same grazing angles as the reflected arrival modified DAE cannot work, while GAME compensates by substituting a subsequent arrival for the reference ray. Another problem exists: the reference arrival must be densely sampled near grazing angles where BTL or SDL change abruptly (e.g. near 40 and 55 degrees for BTL in this study, shown in Figures 5.9a and 5.9b). Although lacking in versatility, modified DAE is functionally equivalent to GAME if reliable direct arrival energy-flux densities are available at all the right grazing angles.

Modified DAE may not be appropriate for borehole data, however. In Section 5.2 the energy-flux densities of direct wave arrivals (1WW) are found to be relatively stronger than those of the reflected wave arrivals (2WW, 3WW, etc.), indicating that it may not be proper to use the direct water wave arrival in borehole data for BRL computations.

3. DATA

3.1 Experiment.

The borehole seismic experiment was conducted on May 26, 1983 at DSDP drill site 581C in the NW Pacific Basin at 43.924 degrees N, 159.7973 degrees E (Figure 1.1). The water is 5467 meters deep at the site. A borehole seismometer was clamped against the side of the hole at a depth of 358 meters below the water/sediment interface and 21 meters into the basalt.

The receiver is comprised of horizontal and vertical geophone arrays in a borehole tool (Duennebier & Blackington, 1983 and Byrne et al., 1986). Two orthogonal pairs of well-matched horizontal geophones and a well-matched vertical geophone stack were used. (The geophones in each orthogonal set were wired in series.) Combined with an amplifier, the response is flat to particle velocity from 4.5 to 13 Hertz and flat to displacement from 13 to 50 Hertz (Duennebier, et al., 1986b). The vertical geophone was determined to be within 5 degrees of true vertical, one horizontal geophone was measured to be about 4 degrees from horizontal and the other within one degree of true horizontal (Duennebier, et al., 1986b). These deviations from true vertical and horizontal will have no significant effect on this study. The azimuthal orientation of the y-axis horizontal geophone (in a right-handed coordinate system) is +89 degrees measured clockwise from north, plus or minus 1.5 degrees (Anderson, et al., 1986). The data were digitized

with 130 dB of dynamic range and a Nyquist frequency of 50 Hz before being transmitted to the ship and recorded.

The sources were two ounce S.U.S. (Sources of Underwater Sound) practice depth charges (P.D.C.'s) set to explode at a depth of 18 meters. The charges were dropped every 40 seconds (every 4 km) from a Navy aircraft. The shot line began about 120 km east of the hole and continued to a point about 20 km west of the hole. The data used in this study were from the shots dropped from 0 to 90 km east of the hole (indicated by the dark solid line in Figure 3.1).

Figure 3.2 displays a spectrogram of the data recorded by the vertical geophone stack during the experiment. In this figure the shots appear as broken vertical lines across a range of frequencies. The single-frequency, horizontal lines may be propeller noise from nearby ships. The strong, persistent, low frequency signature beginning just after shot number 55 is a magnitude 7.7 earthquake, located 15.7 degrees from DSDP site 581C, under the Japan Sea (Duennebier, et al., 1986b). The bottom reflection loss experiment was terminated because of the earthquake.

3.2 Environment.

In the region of the experiment the ocean has a mean depth of about 5400 m. The water depth is assumed constant, since the bathymetry under the shotline varies by less than 100 meters (Figure 3.1). The assumed seawater sound velocity structure is given in Table I (from

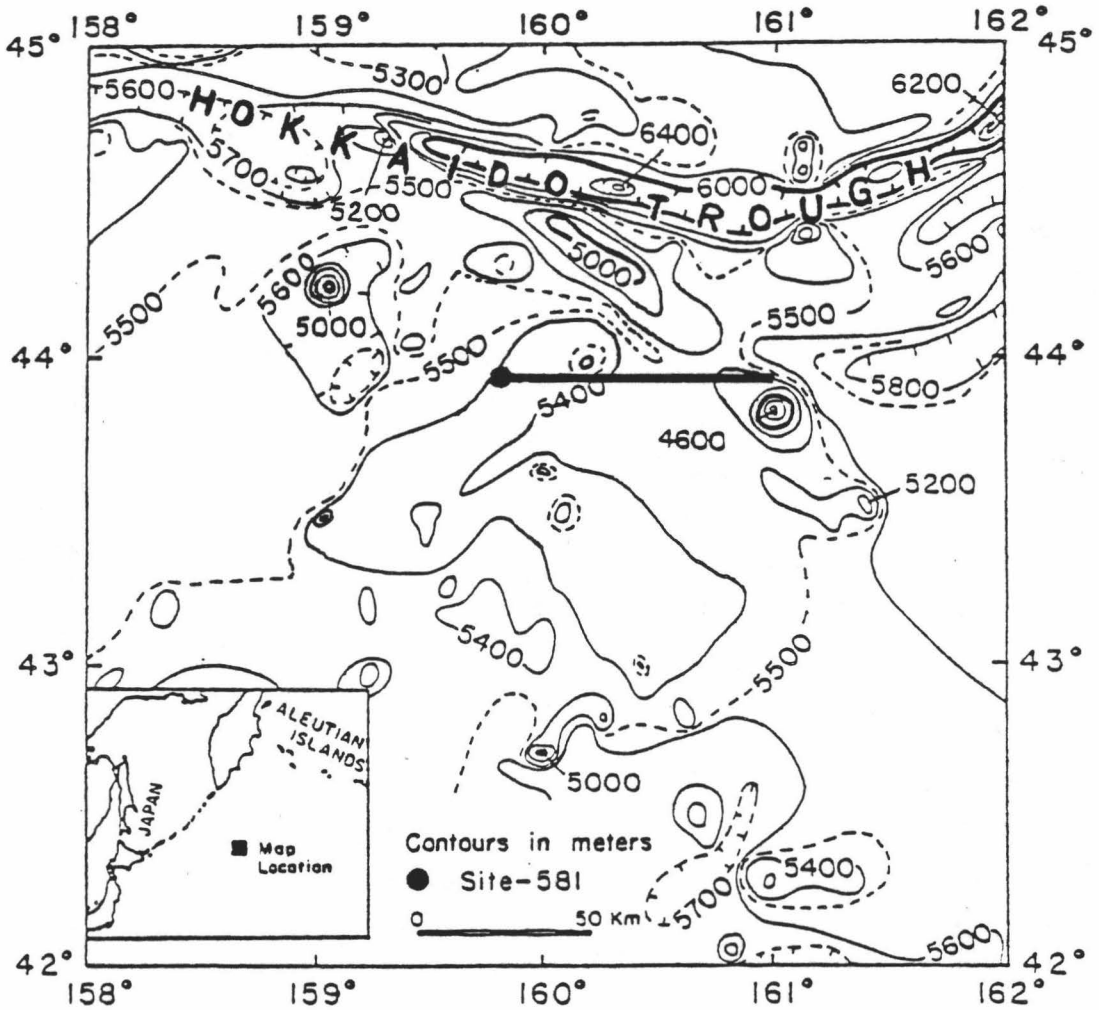

Figure 3.1 Bathymetry in the vicinity of the borehole. The location of the borehole is identified with a solid circle. The locations of shots used in this study are indicated by the solid, heavy line to the east of the hole. (Modified from Bibee and Bee, 1986.)

Figure 3.2 Spectrogram of the borehole seismometer vertical geophone record during the time of the BRL experiment. The y-axis is frequency and the x-axis is time or shot number. Relative signal strength is shown by shading (black is strongest, white is weakest).

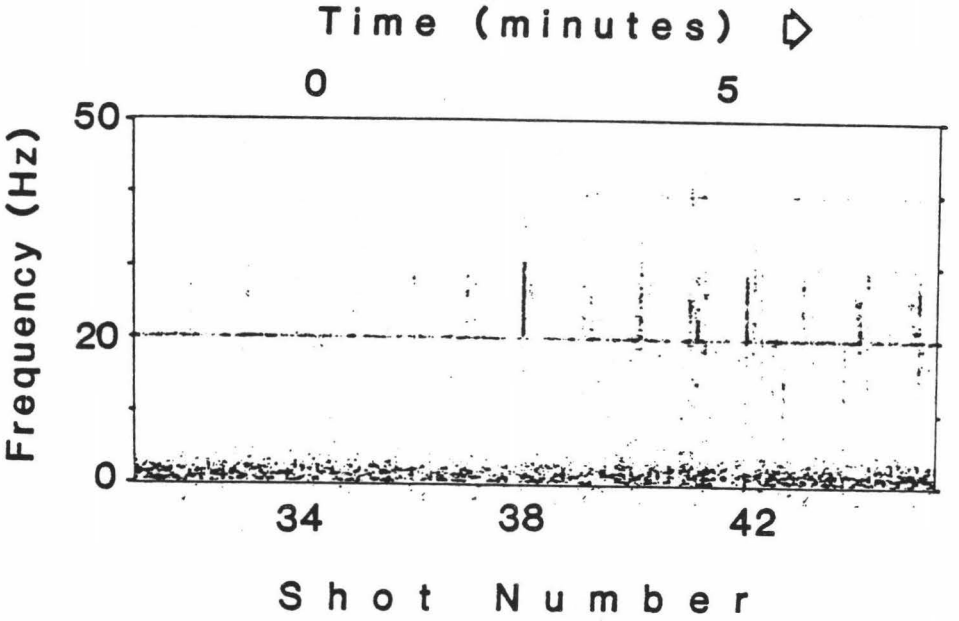
Time (minutes)
0
5
50
20
0
Frequency (Hz)
34
38
42
Shot Number

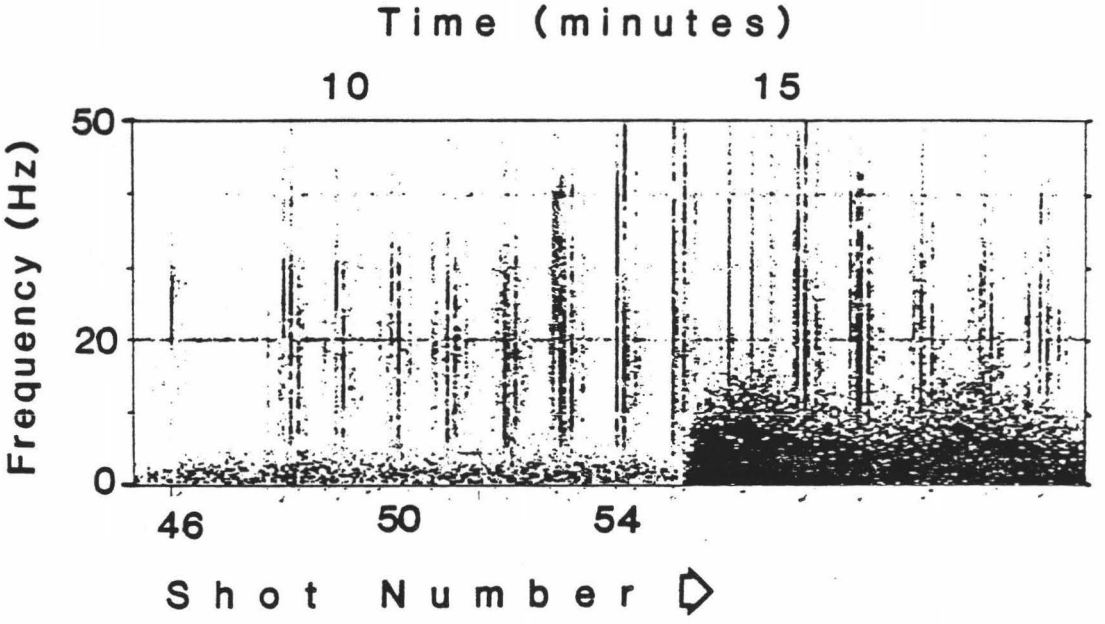
Time (minutes)
10
15
50
20
0
Frequency (Hz)
46
50
54
Shot Number

TABLE I Physical Properties of model.

Depth (meters)	V_p (km/s)	V_s (km/s)	Rho (g/cm^3)	Material
000	1.525	0.0	1.05	SEAWATER
018	1.492	0.0	1.05	"
268	1.483	0.0	1.05	"
393	1.481	0.0	1.05	"
518	1.480	0.0	1.05	"
768	1.482	0.0	1.05	"
1,018	1.492	0.0	1.05	"
2,018	1.506	0.0	1.05	"
3,018	1.524	0.0	1.05	"
4,018	1.542	0.0	1.05	"
4,818	1.552	0.0	1.05	"
5,318	1.570	0.0	1.05	"
5,518	1.580	0.1	1.06	SEDIMENT
5,568	1.600	0.2	1.40	"
5,768	1.650	0.3	1.50	"
5,843	4.000	2.0	2.05	BASALT

Urick, 1983; Figure 5.16, curve 4). This model was used to compute the ocean bottom grazing angles and travel path lengths of acoustic water wave arrivals (as explained in Appendix B.4).

The basaltic basement is approximately parallel to the sediment surface in the area, as shown by single channel reflection data from a line directly west of the hole (Figure 3.3). Thus, by Snell's law, the grazing angle of a ray at the water/sediment interface is the same whether the ray reflects from this interface or from the sediment/basalt interface beneath. (The circle in this figure indicates the receiver location.)

Samples of the sediment and basalt from the hole were obtained during drilling. The sediments recovered were pelagic siliceous clays with some chert bands intermixed near the sediment/basalt interface. A physical property model for these sediments is included in Table I (from F. K. Duennebier, 1986, personal communication). This model was used to compute theoretical BRL (as detailed in Section 5.3). The basalts from the upper 20 meters of the basement recovered from the drill hole were found to be typical mid-ocean ridge basalts (MORBs).

In situ seismic velocities of the oceanic lithosphere in the area of the site were obtained from seismic refraction data by Duennebier et al. (1986a). They found the compressional wave velocity of the topmost basalts to be about 4.0 km/s and the shear wave velocity to be about 2.0 km/s there. These velocities were used to compute theoretical BRL of the sediment/basalt interface (elaboration on this is given in Section 5.3).

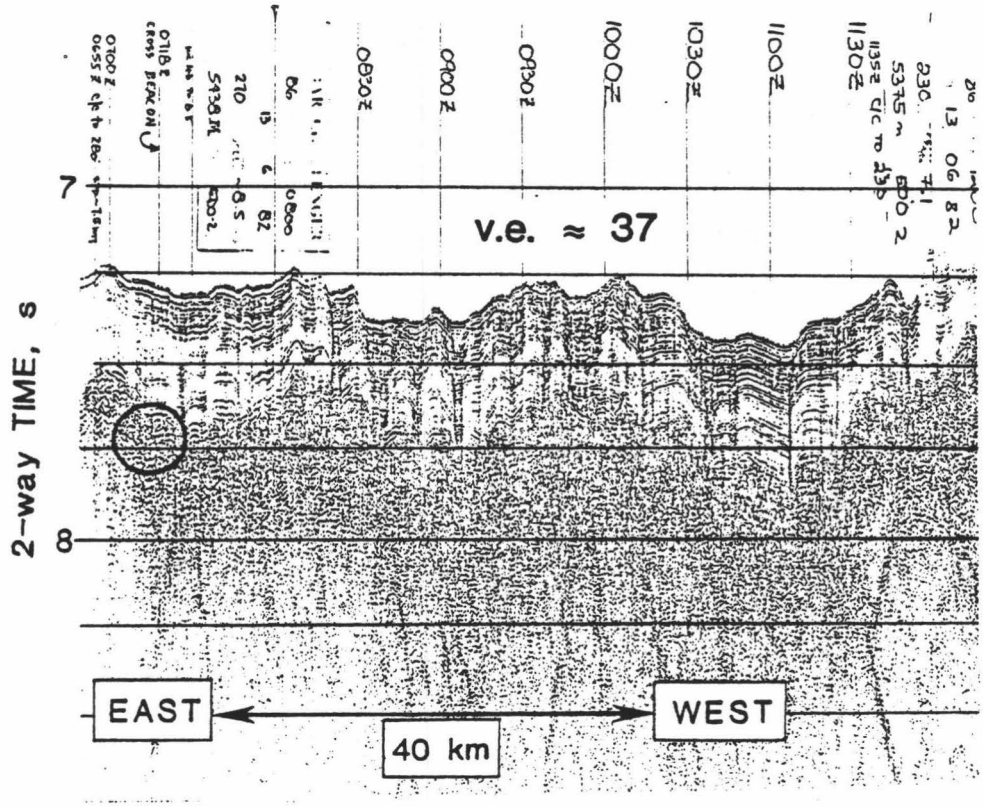

Figure 3.3 Single channel reflection profile west of the borehole. (Modified from Duennebier et al., 1986a and Bibee & Bee, 1986.)

More detailed geophysical data of this area are available in the site survey of Grim & Gettrust (1985). Regional geophysical data and analyses are published in Asada & Shimamura (1976), Anosov et al. (1982) and Bibee & Bee (1986), who also published refraction results at site 581.

3.3 Raw data.

The data samples used in this study are displayed in "waterfall" form in Figure 3.4. The data shown are vertical particle motions. Each trace is aligned so the second eigenray (2WW) falls perpendicular to the time axis. Shot numbers 34 through 54 were used in this study. The data shown were bandpass filtered from 15 to 45 Hertz using a 3-pole Butterworth filter. Each trace has been multiplied by the same scale factor, chosen to make the noise level visible on all traces (thus vertical component noise is seen to be nearly independent of shot range). Although some trace amplitudes have been truncated in this figure, the data themselves are not clipped. The plot was truncated so all the arrivals in each trace can be seen.

Also shown in Figure 3.4 are arrivals from shots fired to the west of the receiver. Although not used in this study, the relative times of the latter arrivals establish the consistency of the arrival time structure of the shots we did use. (Details about the picking of arrivals are given in Appendix B.1.) Noise samples were picked from the record farthest to the left. At close ranges head wave arrivals can be

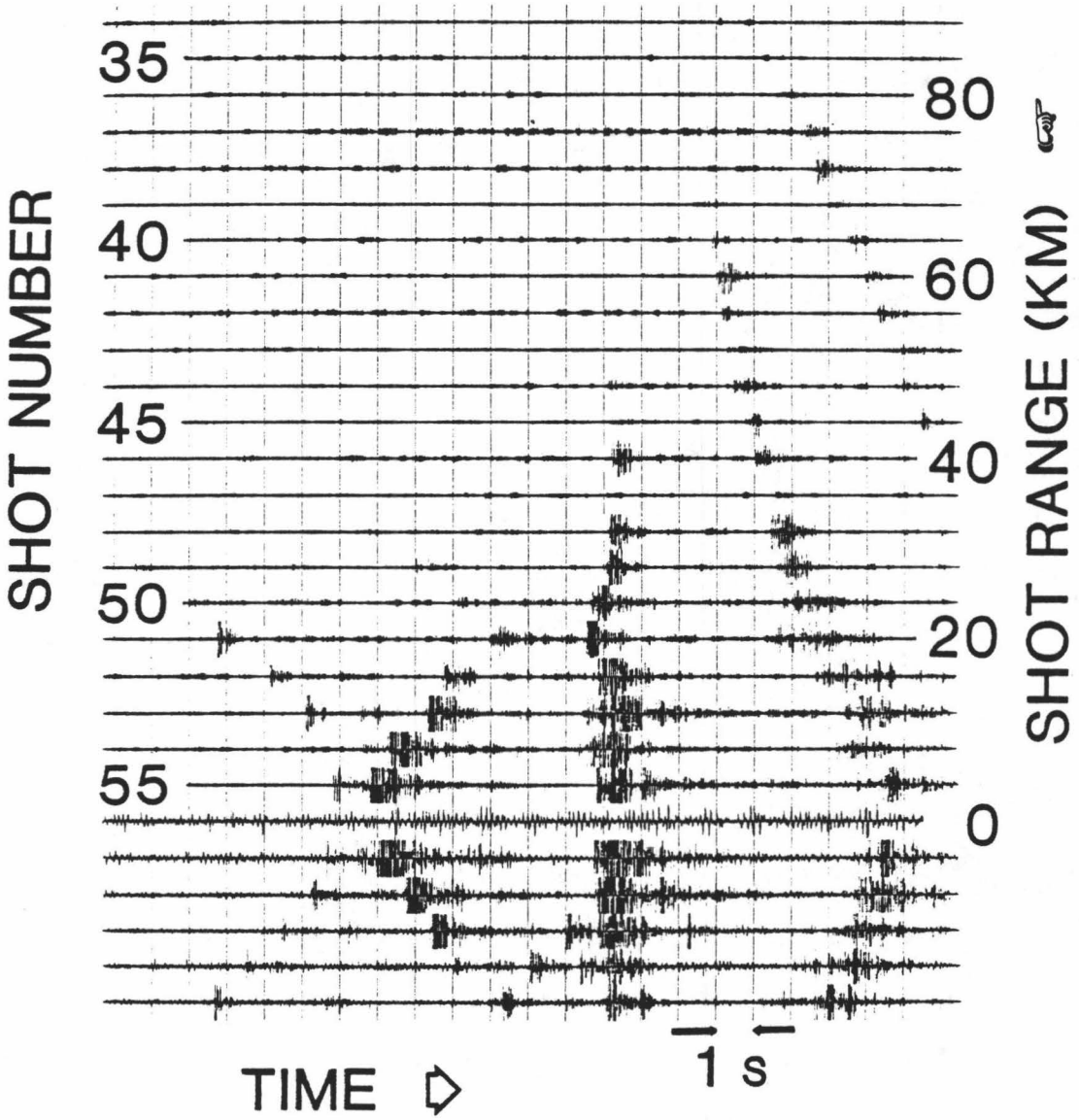

Figure 3.4 Time domain "waterfall" presentation of the data versus shot range. The origin of each trace has been moved to align the second water wave (2WW) arrival in a line perpendicular to the time direction.

seen, prior to the stronger acoustic water wave arrivals. At larger shot ranges head waves become indistinguishable from the noise.

In this experiment the receiver was below the ocean bottom. For the general case of an explosive source in the ocean there are four families of acoustic water waves (Ewing & Worzel, 1948). The eigenrays with one bottom-interaction are illustrated in Figure 3.5. The acoustic water waves recorded in this borehole experiment were downgoing at the receiver (Figures 3.5b and 3.5d). Since the source in this experiment was near the surface and low frequencies were studied, these two arrivals interfered and appeared to be a single arrival, making eigenray identification an easy task (that is, instead of four distinct arrivals with a single bottom-interaction at each range as Figure 3.5 shows, in this experiment only one such arrival was visible).

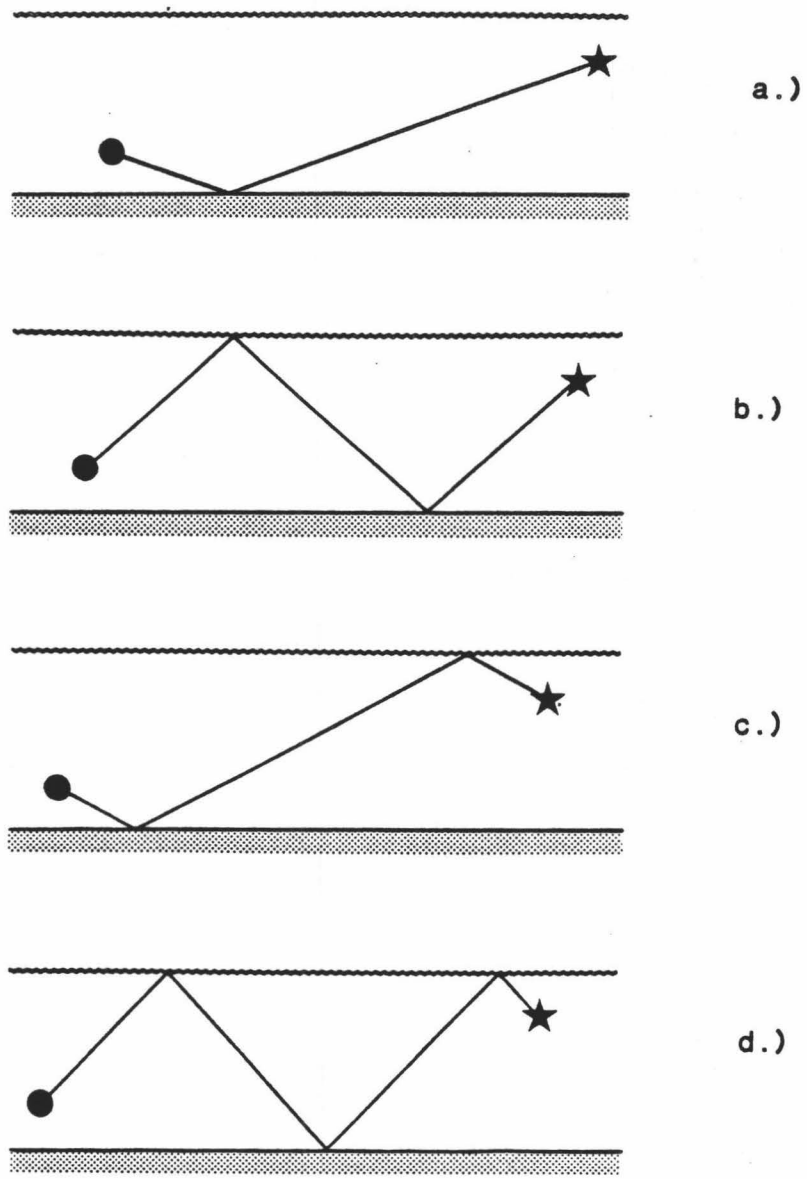

Figure 3.5 The four possible families of bottom-interacting rays in ocean acoustics: a.) Rays downgoing at the source and upgoing at the receiver. b.) Rays downgoing at both the source and receiver. c.) Rays upgoing at both the source and receiver. d.) Rays upgoing at the source and downgoing at the receiver.

4. A GAME ALGORITHM.

Briefly, the algorithm used to implement GAME on the data set at hand is as follows:

1.) Identify and classify the eigenrays according to the number of bottom interactions each has experienced (i.e. the "order" of the rays).

2.) Calculate the energy-flux density of each arrival in a frequency band.

3.) Remove spherical spreading loss over the travel path length of each eigenray.

4.) Calculate the ocean bottom grazing angle (at the water/sediment interface) of each eigenray.

5.) Calculate and apply the correction for surface decoupling loss.

6.) Interpolate the corrected energy-flux density of each arrival order at integer grazing angles between the maximum and minimum angles available in the data set for that order.

7.) Compute energy-flux density ratios using the reference arrival and succeeding arrivals at each interpolated grazing angle.

8.) Normalize the ratios for the difference in the number of bottom bounces of the reflected and reference rays at each grazing angle.

Identical source levels and source depths were assumed for all shots in the experiment.

The eigenray data were tapered and Fourier transformed after step 1 above. After step 2, energy-flux densities estimates of the noise samples were subtracted from the eigenray data to yield the energy-flux density of the eigenray signals. After step 3 energy-flux densities of the signals were averaged over frequency and range. Smoothed signal energy-flux densities were used to compute BRL in this study (via Equation 2.2). They are

$$E(\Delta f,g,J) = [\rho c]\,[t_n - t_1] \sum_{r=r1}^{r2} W_R(r) \sum_{f=f1}^{f2} [W_F(f)\ |X(f,r,J)|^2 \ /\ SDL_a(f,g)\ ]. \qquad (4.1)$$

Here W_R are range smoothing weights (defined in Appendix B.10), W_F are frequency weights (defined in Appendix B.9), X is the frequency domain data, SDL_a is a correction for surface decoupling loss (defined in Appendix B.8), r1 and r2 are the first and last ranges smoothed over, Δf is the frequency band studied, f1 and f2 are the first and last frequencies in the frequency band, and g is grazing angle (determined by range r, ray order J, and the velocity-depth model in Table I). The weights and windows were normalized to preserve the energy in each data sample.

In addition values were interpolated at integer grazing angles by a cubic spline routine (details are given in Appendix B.12). Interpolation was necessary because GAME stipulates that intensity values be known for several arrivals with the same grazing angle, and the data did not fit this requirement.

For each frequency band, and at each grazing angle, the best estimate of BRL is

$$\overline{BRL}(\Delta f,g) = \sum_{J=J1}^{J2} [\ W_{SN}(\Delta f,g,J)\ BRL(\Delta f,g,J)\ ]. \qquad (4.2)$$

This final value is a weighted average of the individual estimates, using the weights, $W_{SN}(\Delta f)$, defined in Appendix B.15. (The entire data processing algorithm is given in Appendix B.)

Because of the frequency weights used in computing energy-flux density (B.2) the quantity (4.1) can be interpreted as a normalized propagation loss, corrected for surface decoupling loss. In the following section (containing intermediate results) propagation loss is presented as a function of shot range (in Figures 5.3a and 5.3b) and of ocean bottom grazing angle (in Figures 5.4a and 5.4b).

5. RESULTS AND DISCUSSION

5.1 Characteristics of the arrivals.

In this study two different components of particle motion were studied: motion in the vertical-radial plane (called PSV motion here) and motion in the transverse horizontal direction (called SH motion here). Both PSV and SH particle motions are generated in the vicinity of the receiver by the same arrival. PSV particle motion is assumed to be composed of both P- and converted SV-wave motion (as expected from a compressional source in a one-dimensional model). If the assumption of one-dimensional structure is true, shot-generated energy should only cause motion in the vertical-radial plane. Any shot-generated energy in the transverse direction (SH particle motion) is caused by secondary phenomena outside the 1-D structure assumption. Examples of structures causing such phenomena are lateral heterogeneity, both of interface structure and sediment or basalt properties, anisotropic materials, and poor coupling of the instrument to the earth.

RMS particle velocities of noise-contaminated acoustic water wave arrivals and ambient noise samples are plotted as a function of shot range for PSV and SH motion in Figures 5.1a and 5.1b, respectively (computed from raw data using Equation A.12, the filter function in Equation B.1, and the mean-square particle velocity transfer function in Table II). Note that SH particle motion for water wave arrivals is 5 to 10 dB less than the corresponding PSV values, justifying the assumption

Figure 5.1 RMS particle velocity (spectrum level) of water wave arrivals and noise samples. Gaps occur where the shot did not explode, where the signal-to-noise ratio is less than 5 dB and where there were no shots. The notation used in the key is illustrated in Figure 1.2.

a.) Values obtained using particle motion (PSV) in the radial-vertical plane.

b.) Values obtained using particle motion (SH) in the transverse horizontal direction.

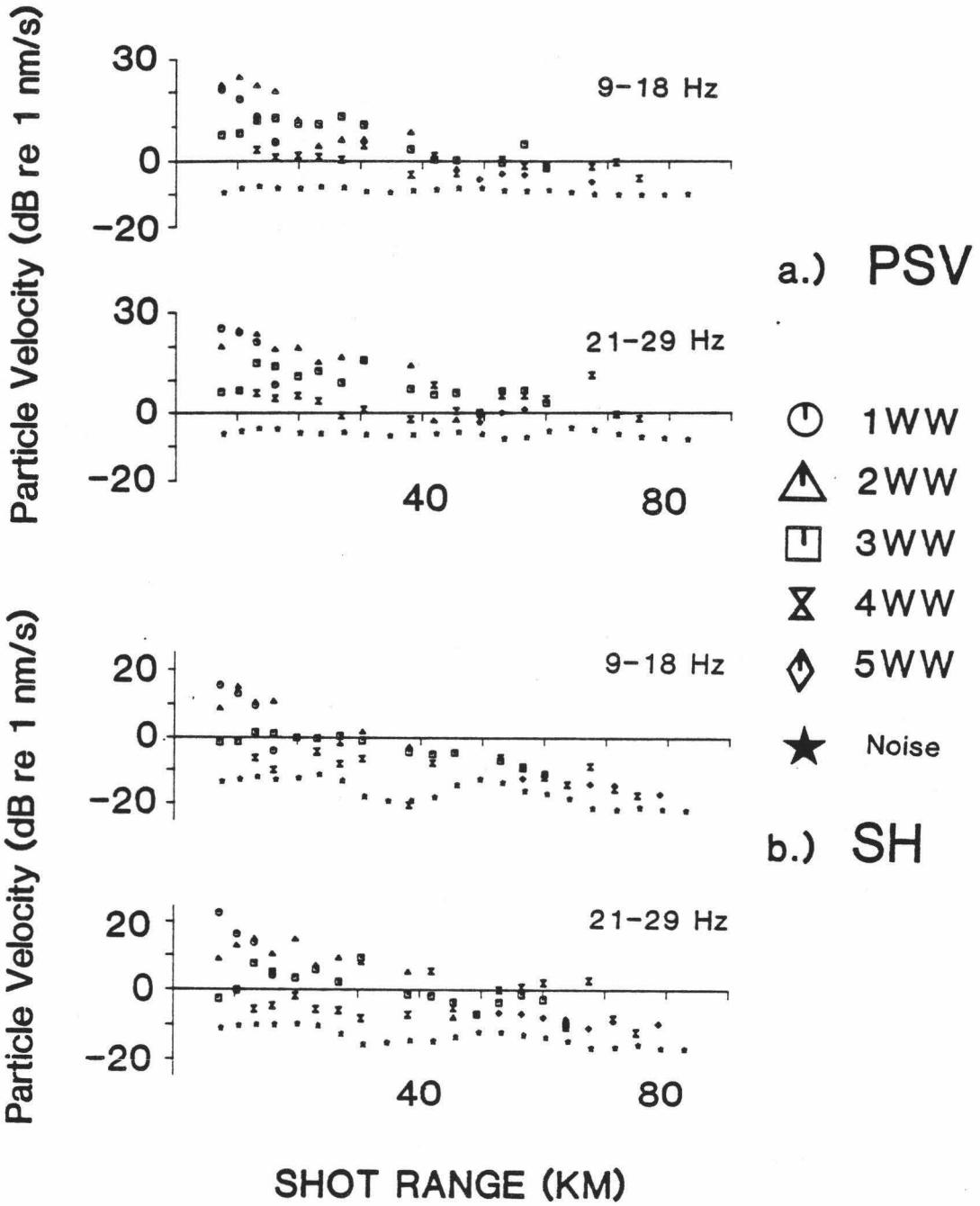
Particle Velocity (dB re 1 nm/s)
30
0
-20
9-18 Hz
21-29 Hz
40
80
a.) PSV
1WW
2WW
3WW
4WW
5WW
Noise
20
9-18 Hz
21-29 Hz
b.) SH
SHOT RANGE (KM)

TABLE II Transfer functions (in dB for a one Hertz bandwidth).

Frequency (Hertz)	Propagation loss	Particle velocity (nm/s)
1.	118.4	28.9
4.	156.2	52.9
5.	162.4	55.9
6.	164.8	56.9
9.	168.5	56.4
13.	170.0	54.7
16.	170.8	53.1
20.	173.6	51.1
22.	174.3	50.2
27.	175.0	48.5
30.	172.0	47.5
50.	153.7	43.2

that phenomena outside a 1-D assumption are of secondary importance. A single channel seismic reflection profile (Figure 3.3) shows nothing unusual in the immediate vicinity of the receiver, implying that these results are not peculiar to the drill site but rather are representative of the survey area. To first order, the interfaces can be assumed to be planar and the layers isotropic and homogeneous.

RMS particle velocities for head wave arrivals are plotted in Figures 5.2a and 5.2b from measured PSV and SH motions, respectively. The values for SH motion are usually lower than the corresponding values for PSV motion; otherwise the two components are similar. Both shear and compressional head wave arrivals are shown. At these frequencies the shear head wave arrivals are stronger than those of the compressional head waves. At some ranges a head wave (2P or 2S) generated by a second order acoustic arrival (2WW) appears stronger than a head wave (1P or 1S) generated by a direct acoustic wave (1WW), a result also observed by Baggeroer, et al. (1984). (This presentation is similar in form to the integrated intensity results given by Bibee & Bee, 1986.)

Comparing the particle motion amplitudes, the head wave arrivals are usually weaker than the water wave arrivals (at the frequencies studied here). There are exceptions in the 9-18 Hertz band. In Figure 5.2a, at 20 km the first compressional head wave (1P) has stronger PSV motion than any water wave arrivals. In Figure 5.2b at 25 km the first shear head wave (1S) has stronger SH motion than the corresponding water wave motions.

Figure 5.2 RMS particle velocity (spectrum level) of head wave arrivals (and noise samples). In the key 1P & 1S stand for the P and S waves generated by the direct water wave, likewise 2P & 2S stand for the P and S waves generated by the second water wave. Gaps indicate that the shot did not explode or that the signal-to-noise ratio is less than 5 dB.

a.) Values obtained using particle motion in the transverse horizontal direction (SH).

b.) Values obtained using particle motion in the radial-vertical plane (PSV).

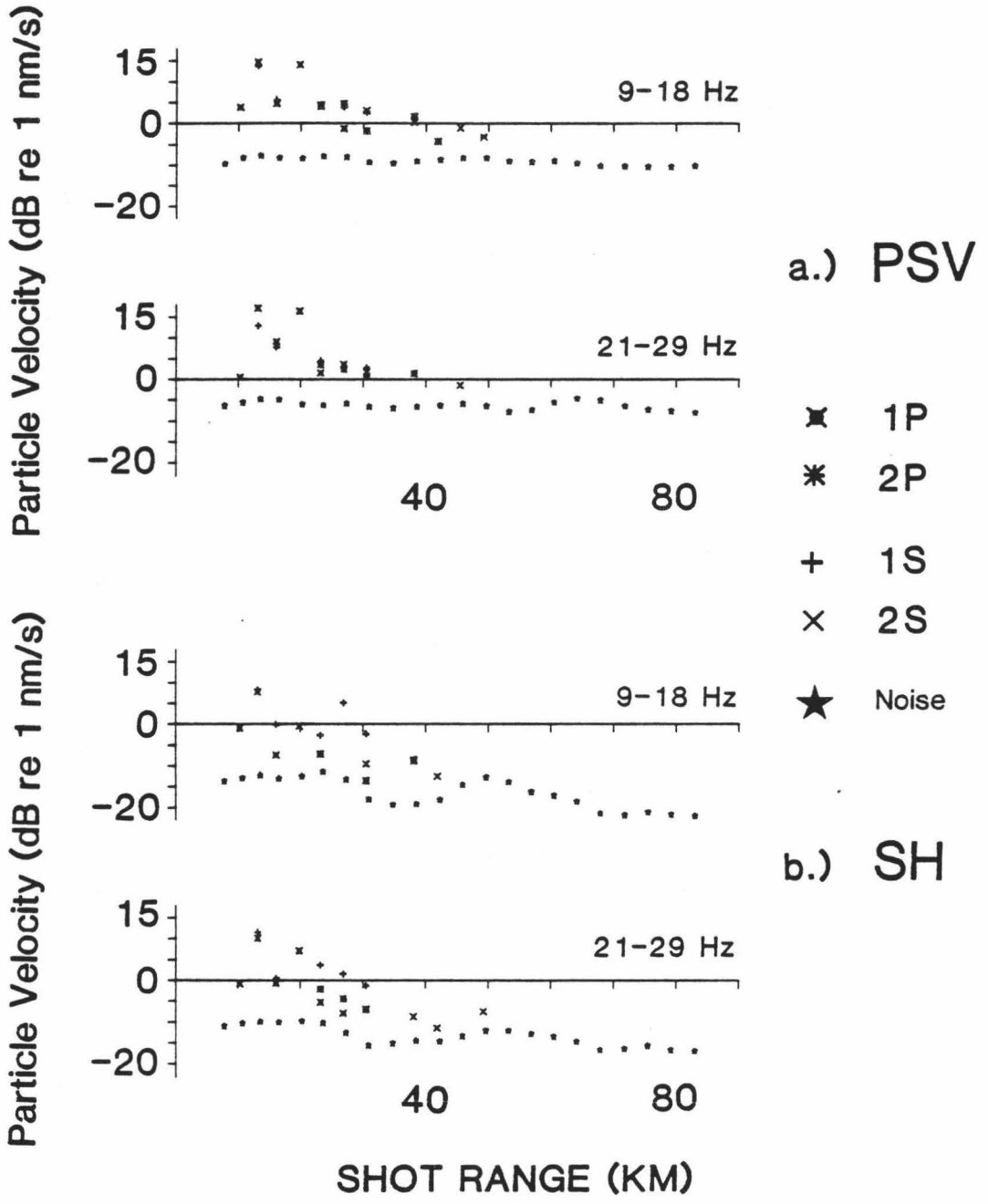
Particle Velocity (dB re 1 nm/s)
15
0
-20
9-18 Hz
21-29 Hz
40
80
a.) PSV
1P
2P
1S
2S
Noise
b.) SH
SHOT RANGE (KM)

In Figures 5.2a and 5.2b the behavior of noise particle motion is clearer than in Figures 5.1a and 5.1b, since there are fewer data points. Notice that the SH noise level is about 5 dB less than the PSV noise level at close range. However, the PSV noise level remains fairly constant over shot range, implying that ambient noise sources dominate (i.e. they are not increased by the arrival of shot-generated energy), while the SH noise level drops with increasing shot range, implying that for those data most noise is shot-generated. This discrepancy can be explained if nearby ships were aligned to the east or west of the receiver, along the azimuth of the shot line. Ships aligned in this way would generate energy in the radial-vertical plane, independent of shot range. For example, Scholte waves on the sediment/basalt interface could generate this motion. In addition, Scholte waves would tend not to be scattered into the transverse horizontal direction. On the other hand, propagating shot-generated sediment reverberations have a greater tendency to be scattered into the transverse horizontal direction (SH). This scattered energy would decrease with increasing shot range (due to geometrical spreading), explaining the observed behavior of SH noise. If the ship-generated noise is stronger than the shot-generated noise, both the PSV and SH noise behaviors match expectations.

5.2 Propagation loss.

Propagation loss of the eigenray signals is plotted, as a function of shot range, for PSV and SH particle motion (in Figures 5.3a

and 5.3b, respectively). (These results were computed using equation 4.1 without the surface decoupling loss term and with SUM in equation B.2 set equal to the sum of the filter taper values.) The signal energy decays more quickly than expected from spherical spreading, and the mean decay of SH particle motion (as $r^{-2.7}$) is greater than that of PSV particle motion (as $r^{-2.5}$). It is interesting to note that 5/2 spreading over the shot range has been predicted when the source is located near an interface (Weston, 1971). (The least squares computations used to determine the spreading exponents employed the algorithm of Menke, 1983.)

Propagation loss is plotted versus ocean bottom grazing angle in Figures 5.4a and 5.4b, after correcting for surface decoupling loss. Notice the sparseness of the direct water wave data compared to data from the other water waves. (The sparseness of the direct water wave data was one reason it was not used in the BRL analysis.)

A smooth curve was drawn through these propagation loss data points after correcting for spreading and surface decoupling loss (Figures 5.5a and 5.5b for PSV and SH particle motion, respectively). In these figures the direct wave (first water wave) curve is higher than the other curves. The difference may be due to the more nearly spherical wavefront of the direct wave compared to the wavefronts of subsequent arrivals. (This is another reason that the first water wave was not used in computing BRL.)

BRL estimates can be found from the difference between the propagation loss (PL) curves of successive order in Figures 5.5a and

Figure 5.3 Propagation loss spectrum level of eigenray signals versus shot range. The notation used in the key is illustrated in Figure 1.2. Gaps occur where the shot did not explode and where the signal-to-noise ratio is less than 5 dB. The solid line is a least squares fit of the data points to the function: r^{-K}, where K is a positive constant. (Also plotted are theoretical spreading curves for K=2 and K=3.)

a.) Values obtained using particle motion in the radial-vertical plane (PSV).

b.) Values obtained using particle motion in the transverse horizontal direction (SH).

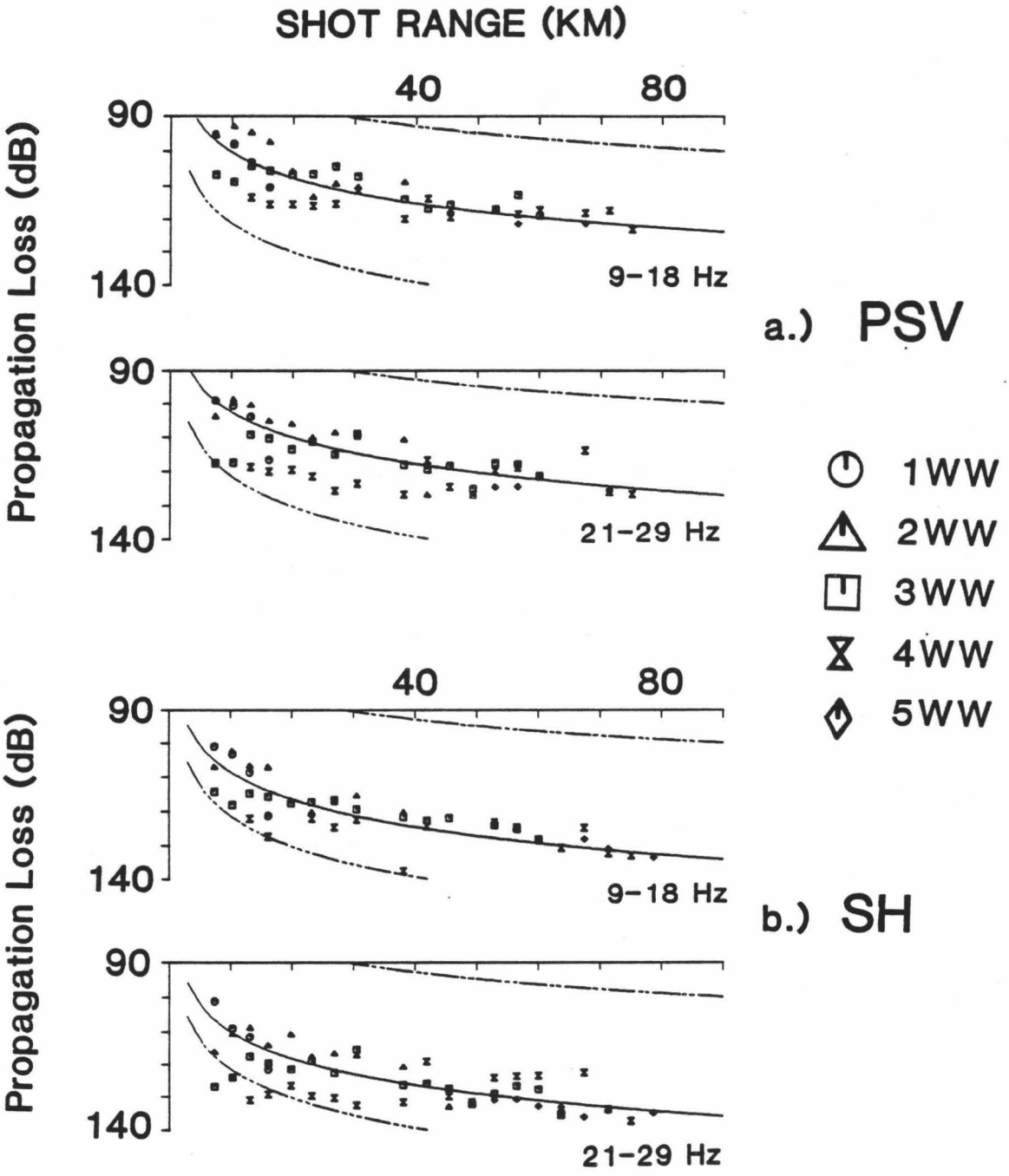
SHOT RANGE (KM)
40
80
90
140
Propagation Loss (dB)
9-18 Hz
21-29 Hz
a.) PSV
1WW
2WW
3WW
4WW
5WW
b.) SH

Figure 5.4 Propagation loss spectrum level of eigenray signals versus ocean bottom grazing angle. The notation used in the key is illustrated in Figure 1.2.

a.) Values obtained using particle motion in the radial-vertical plane (PSV).

b.) Values obtained using particle motion in the transverse horizontal direction (SH).

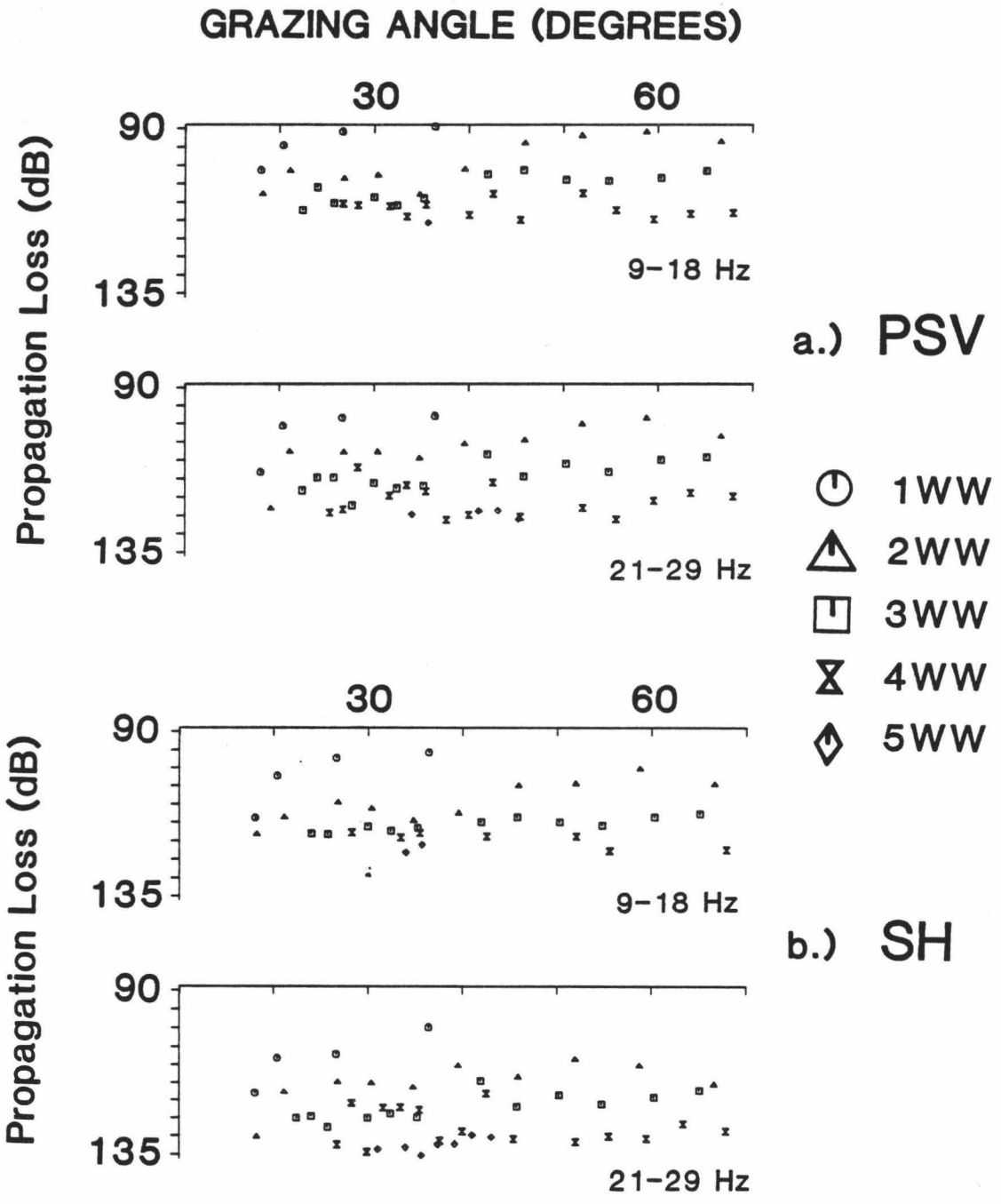
GRAZING ANGLE (DEGREES)
30
60
90
135
Propagation Loss (dB)
9-18 Hz
21-29 Hz
a.) PSV
1WW
2WW
3WW
4WW
5WW
b.) SH

Figure 5.5 Smoothed and corrected propagation loss (spectrum levels) versus ocean bottom grazing angle. The notation used in the key is illustrated in Figure 1.2.

a.) Values obtained using particle motion in the radial-vertical plane (PSV).

b.) Values obtained using particle motion in the transverse horizontal direction (SH).

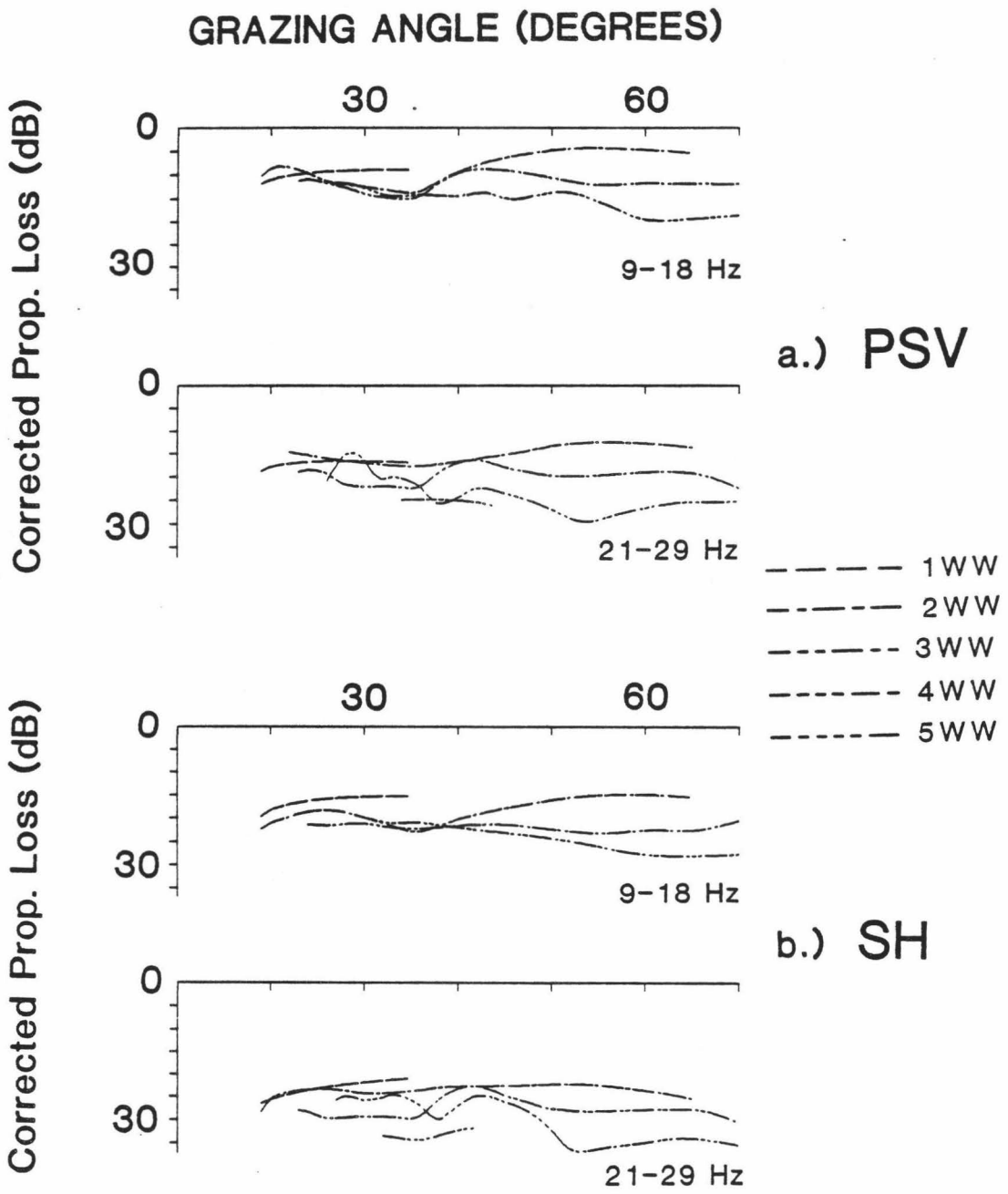
GRAZING ANGLE (DEGREES)
30
60
0
30
Corrected Prop. Loss (dB)
9-18 Hz
21-29 Hz
a.) PSV
1WW
2WW
3WW
4WW
5WW
b.) SH

5.5b. BRL (at grazing angle g) can be estimated from a ray of order N, using the PL curve of order N (at grazing angle g) as the reflected value and the value (at the same grazing angle) of the next lowest curve as the reference value. A more consistent estimate of BRL is found when the reference value is always from the lowest order PL curve. (This latter procedure was used to compute the BRL results given in the following section. As an example of this procedure: In the 9-18 Hz band, at a grazing angle of 50 degrees the order of the reference value is two, this value is matched with the reflected values of order three and of order four.)

By inspecting the propagation loss (PL) plotted in Figures 5.5a and 5.5b the bottom transmission loss, BTL, can be estimated also. BTL is simply the curve for the first water wave arrival, since this arrival has no bottom reflections and other losses have been corrected. Note, however, that the first order eigenray was not recorded at all angles. To obtain BTL estimates over a greater range of grazing angles, and to obtain redundant measurements, BTL can be computed by comparing the PL of the first arriving eigenray (of order greater than one) with the PL of subsequently arriving eigenrays. (This is similar to the preferred BRL computation method mentioned above.)

5.3 Bottom Reflection Loss.

Bottom reflection loss (BRL) estimates computed using PSV and SH particle motion are shown in Figures 5.6a and 5.6b, respectively.

Figure 5.6 Bottom reflection loss (BRL). The symbols used in the key indicate the number of bottom bounces of the reflected ray (of order N in Equation 2.2).

a.) Results obtained using particle motion in the radial-vertical plane (PSV).

b.) Results obtained using particle motion in the transverse horizontal direction (SH).

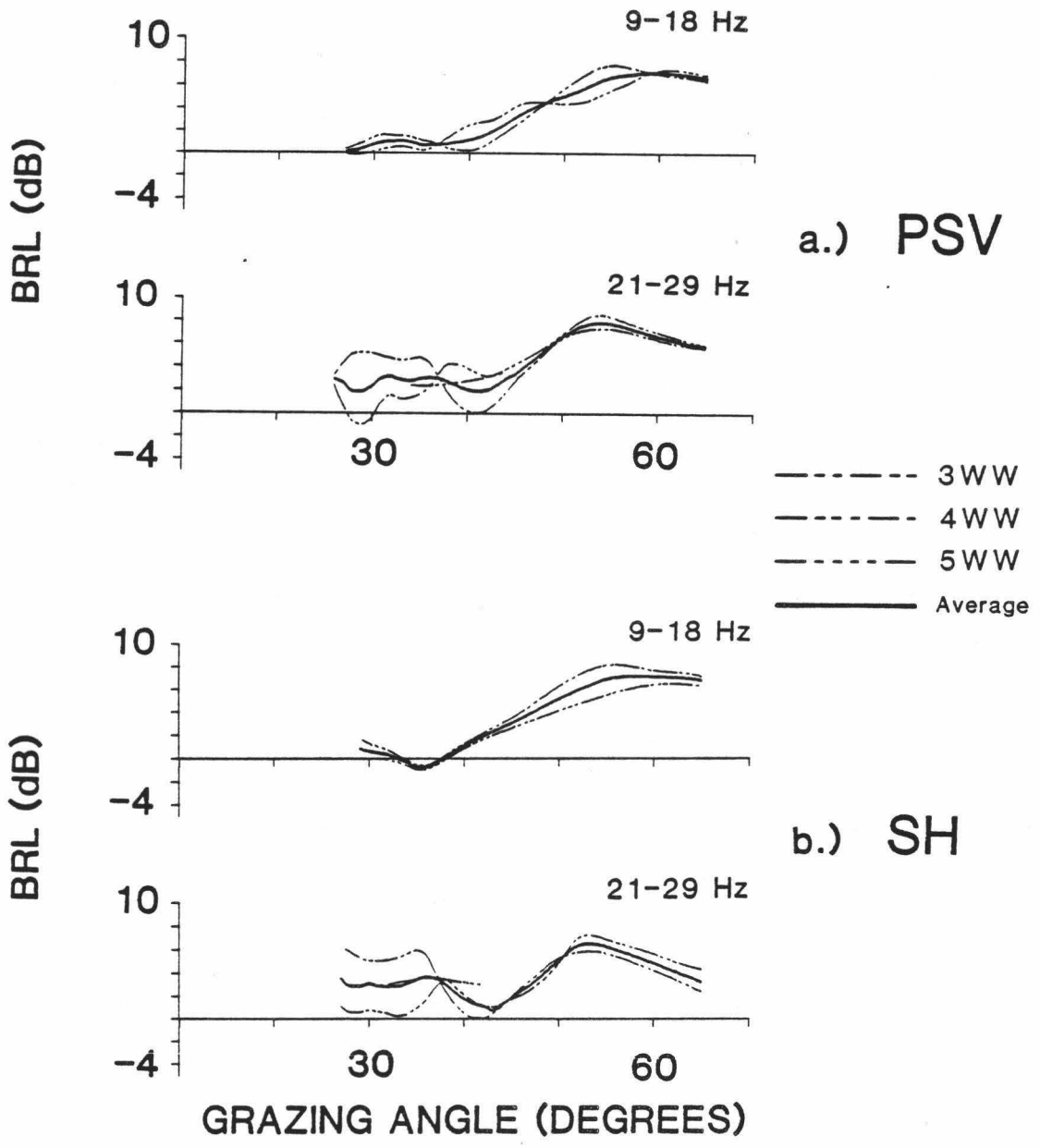
9-18 Hz
10
-4
BRL (dB)
a.) PSV
21-29 Hz
10
-4
30
60
3WW
4WW
5WW
Average
9-18 Hz
10
-4
BRL (dB)
b.) SH
21-29 Hz
10
-4
30
60
GRAZING ANGLE (DEGREES)

BRL results using these two particle motions are similar. The 9-18 Hz band has yielded more consistent results than the 21-29 Hz band. But even so, all the results here are within 3 dB of the mean. The greatest scatter in the data is at low grazing angles.

The results primarily describe the sediment/basalt interface, rather than the water/sediment interface. Plane wave BRL (ignoring multiples) was computed for these two interfaces using a model of homogenous isotropic layers (Table I). Compressional wave reflection and transmission coefficients (energy ratios) were calculated using the algorithm of Aki & Richards (1980). The product of up- and down-going transmission coefficients for the interfaces above the reflector was multiplied by the downgoing reflection coefficient of the reflector interface itself, yielding a total model reflection coefficient. Minus ten times the common logarithm of this coefficients results in the theoretical BRL estimate. The results are shown in Figure 5.7. The figure shows that the strongest specular reflection is expected from the sediment/basalt interface at the angles represented by our data (ocean bottom grazing angles of 28 to 65 degrees). Specular reflections from the water/sediment interface should be at least 20 dB weaker than those from the sediment/basalt interface at these angles.

The empirical BRL results (Figures 5.6a and 5.6b) show a loss minimum near a grazing angle of about 40 degrees. The onset of a BRL minimum has been seen by others to coincide with the emergence of head wave arrivals into the data window (Stickler, 1977; Santaniello, et al., 1979; Chin-Bing et al., 1982). In the results presented here a shear

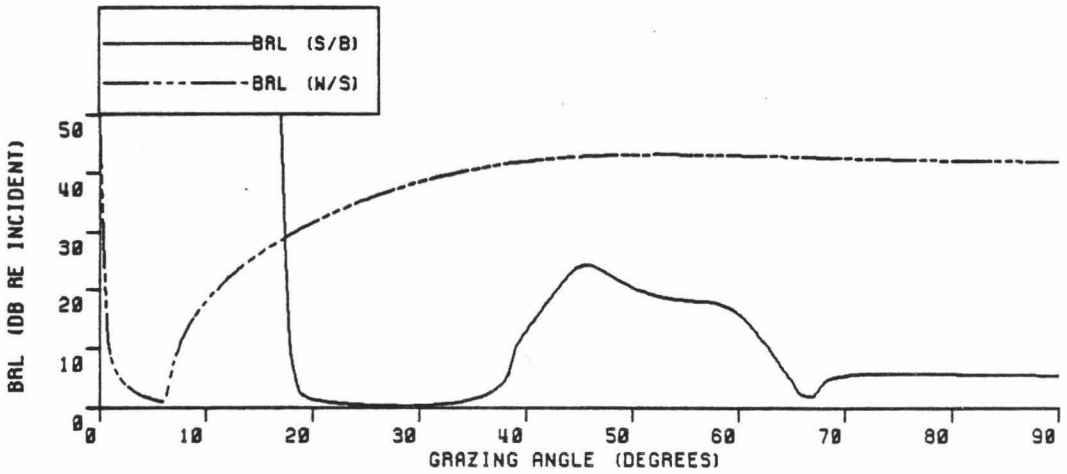

P-WAVE INCIDENT

Figure 5.7 Theoretical plane-wave bottom loss for the water/sediment (W/S) and sediment/basalt (S/B) interfaces.

head wave arrival enters the water wave data window (e.g. at a shot range of about 4 km in Figure 3.4, the first shear head wave arrival emerges and interferes with the direct water wave). The shear wave phase velocity at the receiver depth in the upper oceanic crust can be determined from this information (Burnett et al., 1984). The indicated shear phase velocity is about 2.0 km/s. The minima of all the BRL estimates are not precisely aligned at one grazing angle; possible causes of this discrepancy include lateral heterogeneity in the upper basement velocity structure (White, 1979) and ocean-bottom slope (Itzikowitz et al., 1983 and Koch et al., 1983).

In Figure 5.8 some BRL results obtained here with GAME are compared with two different results computed by S-E. The S-E results were computed with data from other deep ocean sites. They are very similar to the GAME results. Note, however, that the BRL minimum near 40 degrees seen in the GAME result is not seen in the other two results. This may be due to differences in ocean bottom structure, or it may be because they were computed without matching grazing angles. If they used a grazing angle matching method employing empirical arrivals, maybe they would have resolved this BRL feature.

5.4 Bottom Transmission Loss.

BTL estimates using PSV and SH particle motions are presented in Figures 5.9a and 5.9b. The consistency of the BTL results is comparable to that of BRL, seen by the small scatter in the data. In

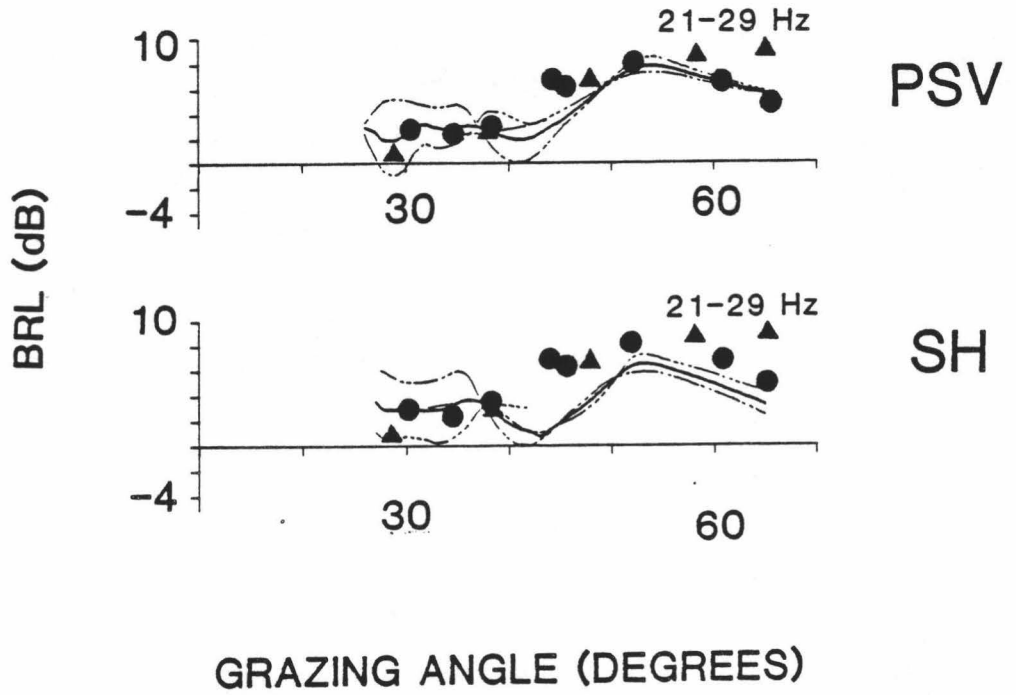

Figure 5.8 Comparison of BRL from this study (using GAME) with results obtained elsewhere using S-E. The triangles are for a band centered on 25 Hz (from Focke, et al., 1980). The dots are for a one-third octave band centered on 40 Hz (from Chapman, 1983).

Figure 5.9 Bottom transmission loss (BTL). The symbols used in the key (NWW) indicate the order (N) of the water wave used to obtain that curve (N and NWW are from Equation B.5). The heavy line is the weighted average of the curves from the individual results.

a.) Results obtained using particle motion in the radial-vertical plane (PSV).

b.) Results obtained using particle motion in the transverse horizontal direction (SH).

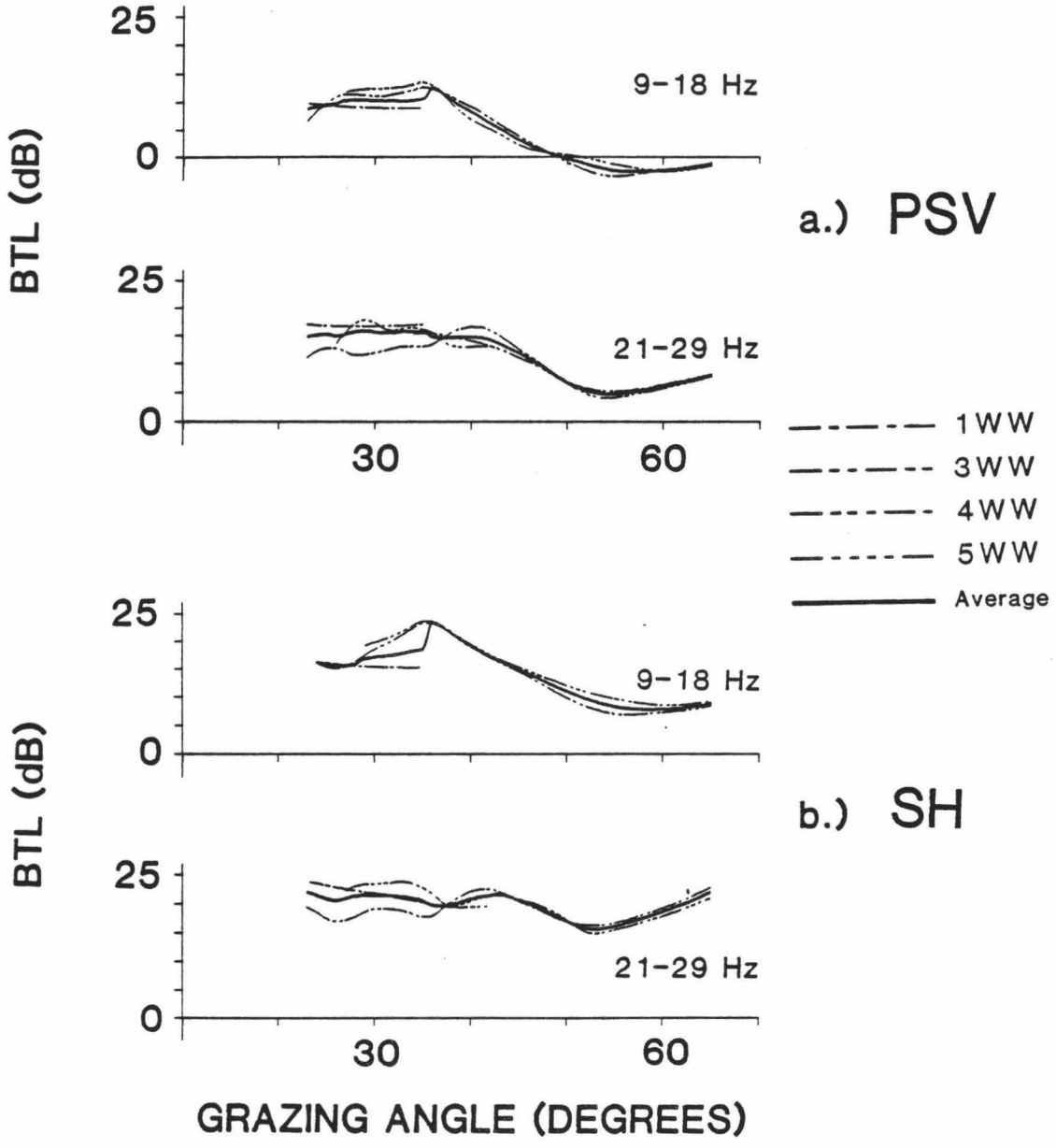
25
0
9-18 Hz
a.) PSV
25
0
21-29 Hz
30
60
BTL (dB)
1WW
3WW
4WW
5WW
Average
25
0
9-18 Hz
b.) SH
25
0
21-29 Hz
30
60
BTL (dB)
GRAZING ANGLE (DEGREES)

addition, BTL (independently) estimated from the first eigenray is consistent with the other estimates.

BTL computed with SH particle motion is quite different from that computed with PSV particle motion. These two results are closer at low grazing angles than they are at higher grazing angles. Whatever mechanism generates the observed SH particle motion, it must be more efficient at low grazing angles than at high grazing angles (at least within the range of grazing angles contained in this data).

The kind of energy observed at each grazing angle can be determined using Snell's law, the seawater acoustic velocity just above the ocean bottom and the upper crustal shear and compressional wave velocities. For grazing angles greater than 70 degrees both P and S waves are propagating. For grazing angles from 40 to 70 degrees, S waves are propagating and P waves are evanescent. For grazing angles less than 40 degrees both P and S waves are evanescent. Significant evanescent energy in the subbottom from acoustic water waves has been predicted in a theoretical study (Stephen, 1984).

BTL depends on grazing angle, expecially between the angles of 40 and 55 degrees. Recall that BTL affects borehole measurements of the acoustic field in the ocean. To compute BRL from borehole data, BTL must first be removed. GAME correctly accounts for the grazing angle dependence of BTL and implicitly removes it.

6. SUMMARY

Bottom reflection loss (BRL) computation methods were classified by the way they estimate incident intensity. A new technique, the grazing angle matching empirical method (GAME), estimates incident intensity using an eigenray arrival with the same grazing angle and frequency as the corresponding reflected ray, but with fewer bottom bounces. GAME was compared and contrasted theoretically with other methods, and was found to be applicable to a greater variety of sources and receivers than the other methods. In particular, computing BRL from borehole data requires a grazing angle matching method.

GAME was applied to a borehole data set to compute redundant and consistent BRL estimates for ocean bottom grazing angles from 28 to 65 degrees. This BRL curve yields an upper crustal shear wave velocity estimate of 2.0 km/s. The BRL values obtained here are similar to those reported by two other workers using another technique and different data.

A new parameter, bottom transmission loss (BTL), was also computed from the data. Consistent results (-5 to +20 dB) were obtained for ocean bottom grazing angles from 24 to 66 degrees. This quantity presents a new perspective on acoustic interaction with the ocean bottom. For example, BTL can be used to better understand propagation loss measured with a borehole receiver (Duennebier, et al., 1986b).

REFERENCES

Anderson, P. N., F. K. Duennebier and R. K. Cessaro, "Horizontal seismic sensor orientation, in an ocean borehole, determined from explosive charges," J.G.R., in press (1986).

Anosov, Gennady I., V. V. Argentov, H. S. Gnibidenko, "Crustal low-velocity zone south of Shatsky Rise, Northwest Pacific Ocean," Geomarine Letters 2, pp. 17-21 (1982).

Asada, T. and H. Shimamura, "Observations of earthquakes and explosions at the bottom of the western Pacific: Structure of the oceanic lithosphere revealed by Longshot Experiment," AGU Monograph 19, pp. 138-153 (1976).

Baggeroer, A., G. Duckworth and R. Stephen, "On the relative amplitudes between primary and multiple signals from seismic refractions in oceanic crust," (abstract) EOS, Transactions of the American Geophysical Union 65, p. 1012 (1984).

Ballagh, K. O., "Limitations to the measurement of sound power by the reference sound source method," J.A.S.A. 72, pp. 1637-1639 (1982).

Bannister, R. W. and M. A. Pedersen, "Low-frequency surface interference effects in long-range sound propagation," J.A.S.A. 69, pp. 76-83 (1981).

Bibee, L. D. and M. Bee, "A seismic refraction study of Cretaceous oceanic lithosphere in the northwest Pacific Ocean," Submitted to J.G.R. (1986).

Brocher, T. M. and R. A. Phinney, "Inversion of slant stacks using finite-length record sections," J.G.R. 86, pp. 7065-7072 (1981).

Bucker, H. P., J. A. Whitney, G. S. Yee and R. R. Goodman, "Reflection of low-frequency sonar signals from a smooth ocean bottom," J.A.S.A. 37, pp. 1037-1051 (1965).

Burnett, M. S., J. A. Orcutt and J. S. McClain, "Synthetic modeling of vertical component OBS water wave data," (abstract), EOS, Transactions, American Geophysical Union 65, p.1013 (1984).

Byrne, D. A., D. Harris, F. K. Duennebier, and R. Cessaro, "Technical review of the ocean bottom seismometer system installed in Deep Sea Drilling Project Site 581C, Leg 88," Submitted to Initial Reports of the Deep Sea Drilling Project, 88: Washington (U.S. Government Printing Office, 1986).

Chapman, N. R., "Low frequency bottom reflectivity measurements in the Tufts Abyssal Plain," in Bottom Interacting Ocean Acoustics, edited by W. Kuperman and F. Jensen (Plenum, New York, 1980), pp. 193-207.

Chapman, N. R., "Modeling ocean-bottom reflection loss measurements with the plane-wave reflection coefficient," J.A.S.A. 73, pp. 1601-1607 (1983).

Chin-Bing, S. A., J. A. Davis and R. B. Evans, "Nature of the lateral wave effect on bottom loss measurements," J.A.S.A. 71, pp. 1433-1437 (1982).

Daniels, J. M. and P. J. Vidmar, "Occurrence and acoustical significance of natural gas hydrates in marine sediments," J.A.S.A. 72, pp. 1564-1573 (1982).

DiNapoli, F. R., D. Potter and P. Herstein, "Comparison of synthetic and experimental bottom interactive waveforms," in Bottom Interacting Ocean Acoustics, edited by W. Kuperman and F. Jensen (Plenum, New York, 1980), pp. 225-237.

Duennebier, F. K. and J. G. Blackington, "The ocean subbottom seismometer," in Geyer, R. A. (ed.) Handbook of Geophysical Exploration at Sea: Boca Raton, Florida (CRC Press) pp. 317-332 (1983).

Duennebier, F. K., B. Lienert, R. K. Cessaro, P. Anderson and S. Mallick, "Controlled-source seismic experiment at Hole 581-C," Submitted to Initial Reports of the Deep Sea Drilling Project, 88: Washington (U. S. Government Printing Office, 1986).

Duennebier, F. K., C. S. McCreery, D. Harris, R. K. Cessaro, C. A. Fisher and P. Anderson, "OSS IV: Noise levels, signal-to-noise ratios, and noise sources," Submitted to Initial Reports of the Deep Sea Drilling Project, 88: Washington (U. S. Government Printing Office, 1986).

Ewing, M. and J. L. Worzel, "Long-range sound transmission," in Propagation of Sound in the Ocean, Geol. Soc. Amer. Mem. No. 27 (1948).

Focke, K. C., S. K. Mitchell and C. W. Horton, Sr., "Analysis of deep ocean sound attenuation at very low frequencies," J.A.S.A. 71, pp. 1438-1444 (1982).

Focke, K. C., J. A. Shooter, N. R. Bedford and S. K. Mitchell, "Church Stroke II Cruise 5 PAR/ACODAC Environmental Acoustic Measurements and Analysis (U)," Applied Research Laboratories, U.T. Austin, ARL-TR-79-52 (1980).

Fryer, G. J., "Reflectivity of the ocean bottom at low frequency," J.A.S.A. 63, pp. 35-42, (1978).

Grim, M. S. and J. F. Gettrust, "Geophysical site survey results: Leg 88," Submitted to Initial Reports of the Deep-Sea Drilling Project, 88: Washington (U. S. Government Printing Office, 1986.

Hampton, L., "Acoustic properties of sediments: An update," Rev. of Geophys. 23, pp. 49-60 (1985).

Hampton, L., S. K. Mitchell and R. R. Goodman, "Acoustic bottom loss measurement using multipath resolution," Proceedings of the IEEE EASCON 1978, pp. 235-251 (1978).

Hastrup, O. F., "Digital analysis of acoustic reflectivity in the Tyrrhenian Abyssal Plain," J.A.S.A. 47, pp. 181-190 (1969).

Hastrup, O. F., "Some bottom-reflection loss anomalies near grazing and their effect on propagation in shallow water," in Bottom Interacting Ocean Acoustics, edited by W. Kuperman and F. Jensen (Plenum, New York, 1980), pp. 135-152.

Hawker, K. E., "Influence of Stonely waves on plane-wave reflection coefficients: Characteristics of bottom reflection loss," J.A.S.A. 64, pp. 548-555 (1978).

Hawker, K. E., "The existence of Stonely waves as a loss mechanism in plane wave reflection problems," J.A.S.A. 65, pp. 682-686 (1979).

Hawker, K. E. and T. L. Foreman, "A plane wave reflection loss model based on numerical integration," J.A.S.A. 64, pp. 1470-1477 (1978).

Hawker, K. E., W. E. Williams and T. L. Foreman, "A study of the acoustical effects of sub-bottom absorption profiles," J.A.S.A. 65, pp. 360-367 (1979).

Itzikowitz, S., M. J. Jacobson and W. L. Siegmann, "Deep-ocean ray transmissions over convergent and divergent sloping bottoms," J.A.S.A. 74, pp. 1250-1259 (1983).

Koch, R. A., S. R. Mitchell and S. G. Payne, "Slope propagation: Mechanisms and parameter sensitivities," J.A.S.A. 74, pp. 210-218 (1983).

Menke, W., Geophysical Data Analysis: Discrete Inverse Theory, (Wiley, New York, 1984).

Mitchell, S. K., N. R. Bedford, and G. E. Ellis, "Multipath analysis of explosive source signals in the ocean," J.A.S.A. 67, pp. 1590-1597 (1980).

Mitchell, S. K. and K. C. Focke, "New measurements of compressional wave attenuation in deep ocean sediments," J.A.S.A. 67, pp. 1582-1589 (1980).

Oakley, D. W. and P. J. Vidmar, "Acoustic reflection from transversely isotropic consolidated sediments," J.A.S.A. 73, pp. 513-519 (1983).

Pekeris, C. L., "Theory of propagation of explosive sound in shallow water," in Propagation of Sound in the Ocean, Geol. Soc. Amer. Mem. No. 27 (1948).

Rutherford, S. R. and K. E. Hawker, "Effects of density gradients on bottom reflection loss for a class of marine sediments," J.A.S.A. 63, pp. 750-757 (1978).

Rutherford, S. R., K. E. Hawker and S. G. Payne, "A study of the effects of ocean bottom roughness on low-frequency sound propagation," J.A.S.A. 65, pp. 381-386 (1979).

Santaniello, S. R., F. R. DiNapoli, R. K. Dullea and P. D. Herstein, "Studies on the interaction of low frequency acoustic signals with the ocean bottom," Geophysics 44, pp. 1922-1940 (1979).

Schoenberg, M., "Nonparametric estimation of the ocean bottom reflection coefficient," J.A.S.A. 64, pp. 1165-1170 (1978).

Spofford, C. W., "Inference of geo-acoustic parameters from bottom loss data," in Bottom Interacting Ocean Acoustics, edited by W. Kuperman and F. Jensen (Plenum, New York, 1980), pp. 159-171.

Stephen, R. A., "Finite difference seismograms for laterally varying marine models," Geophys. J. of the Roy. astr. Soc. 79, pp. 185-198 (1984).

Stern, M., A. Bedford and H. R. Millwater, "Wave reflection from a sediment layer with depth-dependent properties," J.A.S.A. 77, pp. 1781-1788 (1985).

Stickler, D. C., "Negative bottom loss, critical-angle shift, and the interpretation of the bottom reflection coefficient," J.A.S.A. 61, pp. 707-710 (1977).

Stoll, R. D. and T. -K. Kan, "Reflection of acoustic waves at a water-sediment interface," J.A.S.A. 70, pp. 149-156 (1981).

Sutton, G. H. and P. W. Pomeroy, "Analog analyses of seismograms recorded on magnetic tape," J.G.R. 68, pp. 2791-2815 (1963).

Tuteur, F. B., "Underwater acoustic scatter channels with several bounces," J.A.S.A. 60, pp. 840-843 (1976).

Urick, R. J., Principles of Underwater Sound, 3rd ed. (McGraw-Hill, New York, 1983).

Vidmar, P. J., "The dependence of bottom reflection loss on the geoacoustic parameters of deep sea (solid) sediments," J.A.S.A. 68, pp. 1442-1453 (1980).

Vidmar, P. J., "The effect of sediment rigidity on bottom reflection loss in a typical deep sea sediment," J.A.S.A. 68, pp. 634-638 (1980).

Vidmar, P. J., "Ray path analysis of sediment shear wave effects on bottom reflection loss," J.A.S.A. 68, pp. 639-648 (1980).

Weston, D. E., "Intensity-range relations in oceanographic acoustics," Journal of Sound and Vibration 18, pp. 217-287 (1971).

White, R. S., "Oceanic upper crustal structure from variable angle seismic reflection-refraction profiles," Geophys. J. of the Roy. astr. Soc. 57, pp. 683-726 (1979).

White, R. S., and R. A. Stephan, "Compressional to shear conversion in oceanic crust," Geophys. J. of the Roy. astr. Soc. 63, pp. 547-565 (1980).

APPENDIX A. Computation of Energy-Flux Density.

Energy-flux density, E, often employed in the formulation of ocean acoustics problems using a broadband source, is defined as the integral of intensity (Urick, 1983, p. 14). For plane waves instantaneous intensity, I, is related to instantaneous pressure, p, by

$$I(t) = p^2(t) \;/\; [\rho c],$$

where c is sound velocity, ρ is density and t is time. Given digital pressure data, energy-flux density, E, can be computed as follows:

$$E = [(t_n - t_1)/(\rho c)]\ [1/n] \sum_{k=0}^{n-1} [\ p^2(t_k)\ ]. \qquad \text{(A.1)}$$

Here k is the time index, n is the number of samples and the sampling rate is assumed to be constant. (E is essentially the mean-square pressure, normalized for the data window length and the impedance of the medium where the receiver is located.)

Assuming plane waves, pressure is related to particle velocity, u, by $p = [\rho c][u]$, Equation A.1 can be rewritten as

$$E = (t_n - t_1)(\rho c)(1/n) \sum_{k=0}^{n-1} [\ u^2(t_k)\ ], \qquad \text{(A.2)}$$

or,

$$E = (\rho c)(t_n - t_1)\ \bar{u}^2, \qquad \text{(A.3)}$$

where $\bar{u}^2$ is the mean-square particle velocity.

The relationship between the digital data values, x(k), and energy-flux density, E, can now be found. The n recorded digital data values can each be expressed in terms of the discrete frequency components X(j) as

$$x(k_o) = [\sqrt{n}/n] \sum_{j=-n/2}^{n/2-1} [\, X(j) \exp(-i2\pi jk_o/n) \,], \qquad (A.4)$$

where k_o is the index of a particular time sample and j is the frequency index. Similarly, each frequency component of the data can be expressed in terms of the time series x(k) by

$$X(j_o) = [\sqrt{n}/n] \sum_{k=0}^{n-1} [\, x(k) \exp(+i2\pi j_o k/n) \,], \qquad (A.5)$$

where j_o is the index of a particular frequency sample. (Equations A.5 and A.4, respectively, define the forward and inverse discrete Fourier transformations, DFT, used in this study.)

Given the time and frequency domain data and the DFT definitions in (A.4) and (A.5), it follows that

$$\sum_{j=-n/2}^{n/2-1} |X(j)|^2 = \sum_{k=0}^{n-1} x^2(k) \qquad (A.6)$$

by the generalized Parseval-Rayleigh theorem (Bracewell, 1978). Since the component, $X(-j_o)$, for each frequency, j_o, is the complex conjugate

of the component, $X(+j_o)$, Equation A.6 can be rewritten as

$$\sum_{j=0}^{n/2} [2/n] \; |X(j)|^2 = \sum_{k=0}^{n-1} [1/n] \; x^2(k), \tag{A.7}$$

where both sides have also been divided by n. Note that the right side of (A.7) is simply the mean-square of the time series. Given the instrument particle velocity transfer function, $F_{PV}(j)$, the mean-square particle velocity is

$$\bar{u}^2 = \sum_{j=0}^{n/2} [\; [2/n] \; |X(j)|^2 \; / \; F_{PV}(j) \;]. \tag{A.8}$$

After substituting the mean-square particle velocity transfer function,

$$F_{MSPV}(j) = [n/2] \; F_{PV}(j), \tag{A.9}$$

we get

$$\bar{u}^2 = \sum_{j=0}^{n/2} [\; |X(j)|^2 \; / \; F_{MSPV}(j) \;]. \tag{A.10}$$

This quantity can be substituted into (A.3) to get energy-flux density from the data:

$$E = [\rho c] \, [t_n - t_1] \sum_{j=0}^{n/2} [\; |X(j)|^2 \; / \; F_{MSPV}(j) \;]. \tag{A.11}$$

Here the X(j) are the output of the DFT used here (A.5) and the $F_{MSPV}(j)$ are the transfer function elements (A.9).

The mean-square particle velocity in some frequency band, rather than all frequencies, can be obtained by filtering the data. If the filter is applied in the frequency domain, the result is:

$$\bar{u}_*^2(\Delta j) = \operatorname*{sum}_{j=0}^{n/2} \left\{ [2/n]\ w(j)\ |X(j)|^2 \ /\ F_{MSPV}(j) \right\} \qquad \text{(A.12)}$$

where w(j) are the filter coefficients and $\bar{u}_*^2(\Delta j)$ is the mean-square particle velocity in the discrete frequency band Δj. (If the filter is a delta function, the resulting filtered time series is monchromatic.)

APPENDIX B. DATA REDUCTION

The algorithm used in this study to reduce the data is outlined below:

B.1 Pick data.

B.2 Deglitch data.

B.3 Determine ranges and azimuths of shots.

B.4 Calculate grazing angles and travel path lengths.

B.5 Correct for spreading.

B.6 Combine geophone outputs for the PSV or SH response.

B.7 Isolate the frequencies to study.

B.8 Correct for surface decoupling loss.

B.9 Convolve with the transfer function.

B.10 Pick and apply noise estimates.

B.11 Smooth intensity over adjacent ranges.

B.12 Determine grazing angles and interpolate intensities between measured angles.

B.13 Take ratios to compute BRL.

B.14 Solve equations to compute BTL.

B.15 Compute weighted average of BRL or BTL using (signal+noise)/noise (in dB) as weights.

In the following these steps are discussed in detail.

B.1 Data picks made.

The data (discussed in Section 3.3) showed strong arrivals at time intervals appropriate for acoustic water-wave multiples. These are rays which bounce between the ocean bottom and the sea surface (Figure 1.2). These arrivals were analyzed here for bottom reflection loss. Ray tracing is necessary in the more general case, where the source or receiver (or both) are located at mid-depth in the ocean, to identify the eigenray arrivals (Mitchell et al., 1980).

A time average is inherent in BRL computation with broadband sources (Appendix A). In addition, since the computation of BRL was done in the frequency domain, a tapered window should be applied to the time sample before Fourier transformation to reduce leakage error (Bracewell, 1978). The window length used for water wave arrivals and noise samples in this study was 2.56 seconds. (A 1.28 second window was used for the head wave arrivals picked to compare with the water waves.) Hanning windows, aligned so that the highest amplitude portion of the arrival was 2/5 of the way into the window, were used. (The time window is symbolized by WT in Equation 4.1.)

B.2 Deglitch the data.

Some incorrect values were interspersed among the good data, due to a digitization problem. Incorrect data points were recognized as values occuring more than NPTS/30 times in a data window, where NPTS is

the number of points in the data window. These incorrect values were removed and their values approximated by interpolation from adjacent (good) data values using the cubic spline routines IQHSCU and ICSEVU (IMSL, 1984).

B.3 Determine ranges and azimuths of shots

Shot-receiver offsets were calculated from the shot and receiver coordinates. The shot coordinates and times of the drops were given by the U.S. Navy. The shot drop locations were combined with eigenray travel time information to reconstruct the receiver location. The receiver location determined by this method was found to be systematically in error. The error was attributed to a systematic error, possibly involving both the location of both shots and receiver, while the shot line orientation was assumed to be correct. The shot drop coordinates were adjusted (by 1.52 minutes west and 1.90 minutes north) relative to the fixed receiver location to fit expected travel times to the eigenray travel time data. The corrected shot coordinates and known receiver coordinates were used to compute the magnitudes (offsets) and directions (azimuths) of the receiver-to-shot vectors.

B.4 Calculate grazing angles and travel path lengths.

Ray tracing was used to calculate the grazing angle and travel path length for each observed eigenray, assuming specular reflection

from the sediment/basalt interface. (This interface was identified as the strongest seismic reflector in Section 5.3.) An acoustic model of the ocean representative of the experimental site (from Urick, 1983; Figure 5.16, curve 4) was used in the ray tracing computation, with sediment acoustic velocities from Duennebier, et al. (1986a). The sound velocities used are given in Table I. The grazing angle and travel path length assigned to each eigenray were computed using the corrected range of the shot, the number of bounces of the eigenray and the slope of the bottom in the direction of the shot line. Rays were traced iteratively to determine the take-off angle at the source for each arrival such that the range error was less than one meter. The grazing angle at the ocean bottom and sea surface were obtained by Snell's law. The travel path length was computed in conjunction with the eigenray grazing angle determination.

B.5 Correct for spreading.

The eigenray spreading correction used here is

$$Spr_a(J,g) = L^{-2}(J,g)$$

where J is the order, g is the ocean bottom grazing angle and L is the travel path length of the eigenray, assuming a parallel ocean bottom and sea surface. Rays were traced to compute L (ray tracing is discussed in Section B.4). For the regional ocean bottom slope, s, encountered at

this site (where s < 0.5 degree) and the shot ranges, r, in this experiment (where r < 90 km) the parallel approximation will not cause significant errors in the travel path lengths. This correction assumes spherical (ie. inverse squared) spreading along the rays' travel path.

Spreading loss in ocean acoustics is often quantified as some exponential function of shot-receiver offset (e.g. Urick, 1983; p. 102). These spreading laws are approximations based on intensity analysis of eigenray sums, rather than the study of individual eigenray intensities (Weston, 1971). Since individual eigenrays are studied here, the spreading of each eigenray is determined and corrected separately.

B.6 Combine geophone responses to find PSV and SH response magnitudes.

The geophone response magnitudes in the radial and transverse horizontal directions ($|X_{hr}|$ and $|X_{ht}|$, respectively) were computed with data recorded by the oriented horizontal geophones, h1 and h2. (Radial motion is positive towards the shot and transverse motion is positive to the right of the shot-to-receiver vector.) The equations used are

$$|X_{ht}(j)|^2 = |X_{h1}(j)|^2 \sin(A+dA) - |X_{h2}(j)|^2 \cos(A+dA)$$

and

$$|X_{hr}(j)|^2 = |X_{h1}(j)|^2 \cos(A+dA) + |X_{h2}(j)|^2 \sin(A+dA)$$

from Sutton and Pomeroy (1963). Here the X(j) are oriented orthogonal horizontal geophone components (at frequency j) in the directions

indicated by the subscripts (hr, ht, hl and h2), A is the corrected azimuth of the receiver-to-shot vector (see Section B.3) and dA is the azimuth of the hl ("y-axis") geophone (89 degrees East from North). The geophones are discussed in more detail in Section 3.1. The phase lag between the multiplexed geophone channels was corrected before coherently combining the geophone responses.

Motion in the transverse horizontal direction (SH) is

$$|X_{SH}(j)|^2 = |X_{ht}(j)|^2.$$

The horizontal response in the radial direction was combined with the output of the vertical geophone, yielding the vector magnitude in the radial-vertical plane, called PSV motion here:

$$|X_{PSV}(j)|^2 = |X_{hr}(j)|^2 + |X_z(j)|^2,$$

where X_z is the vertical geophone output and the phase lag between the radial and vertical components was corrected before combining them.

B.7 Isolate frequency bands used in this study.

Close examination of the waveforms of the water wave showed aliasing to be present. The frequency bands chosen for analysis were well below the Nyquist frequency to avoid aliasing artifacts. Two frequency bands were chosen (9-18 Hz and 21-29 Hz). The data on either

side of these bands was tapered down to zero over 2.5 Hertz. These tapered data are included in the analysis (this is detailed in Section B.9).

B.8 Correct for surface decoupling loss.

Surface decoupling loss corrections were computed using the linear approximation technique recommended by Bannister and Pedersen (1981). This correction depends both on frequency and the sea surface grazing angle of the upgoing ray at the source (Figure 3.5d).

B.9 Compute average values (with units) in a frequency band.

BRL ratios in (2.2) were computed for average energy-flux density in a frequency band using (4.1) instead of using the discrete frequency energy-flux densities in (A.11). This modification was made to conserve computer storage space and computation time. The BTL ratios computed in this study also utilized the frequency band energy-flux densities in (4.1).

The frequency bands were tapered at the ends. The taper window, w(f), is defined this way:

$$
\begin{aligned}
w(f) &= (1/2)(1+\cos(\pi(f_1-f)/fedge)) &&: (f_1-fedge) < f < f_1 \\
w(f) &= 1.0 &&: f_1 < f < f_2 \qquad \text{(B.1)} \\
w(f) &= (1/2)(1+\cos(\pi(f-f_2)/fedge)) &&: f_2 < f < (f_2+fedge).
\end{aligned}
$$

Here "fedge" is the tapering length of the window on either side of the cut-off frequencies, f_1 and f_2. (In this study, fedge=2.5 Hz.)

The frequency band taper and transfer function combine to give the normalized frequency weights, W_F, used in (4.1):

$$W_F(f) = [\ w(f)\ /\ F_{PL,a}(f)\ ]\ /\ SUM, \tag{B.2}$$

where

$$F_{PL,a}(f) = [\ F_{MSPV,a}(f)\ ][\ E_S(f)\ ]$$

is a transfer function for propagation loss. $F_{MSPV,a}$ and $E_{S,a}$ were defined in Section 2.3 and SUM is the normalizing term. (Transfer functions are given numerically in Table II for a one Hertz bandwidth; since the data samples studied here have a bandwidth of less than one Hertz, they were smoothed over frequency before using the transfer functions.)

When PL or BTL is computed, SUM is the sum of the frequency window elements, w(f), in the band. When BRL is computed, SUM cancels in the ratio. Since it cancels, it can be set equal to anything. If we say SUM is the sum of $[\ w(f)\ /\ F_{PL,a}(f)\ ]$ over the frequency band Δf, then we can think of BRL as a power of the weighted average of E(N) and E(M), where $[\ w(f)\ /\ F_{PL,a}(f)\ ]$ are the weights and the exponent is 1/(N-M).

B.10 Pick and apply noise estimates.

The noise picks were chosen from the data recorded prior to the arrival of the first visible signal from each shot (Figure 3.4). In addition to ambient noise, source-generated noise (e.g. reverberations caused by previous shots) is included in these estimates.

The noise samples were processed in the same way as the signal data. That is the samples were each deglitched and the squared magnitude of the PSV and SH response, in each frequency band and at each range, was obtained.

The noise estimates were used in three ways: 1.) Noise sample mean-square particle velocities were subtracted from the noise-contaminated data at each discrete frequency to recover the mean-square particle velocity of the signals alone, 2.) The signal-to-noise ratio of the eigenray arrivals at each discrete frequency was used as a measure of data reliability to weed out weak arrivals of dubious accuracy (this was done by specifying a critical signal-to-noise value of 3.0 and ignoring any arrival which had a signal-to-noise ratio below this value), 3.) The signal visibility, (signal+noise)/noise, at each frequency and range was summed over a frequency band and used to weight the estimates of BRL or BTL using those signals in the final weighted average for that frequency band.

B.11 Smooth the data points over adjacent ranges.

The particle velocity data at each range were smoothed using data from the adjacent shots (four kilometers away). A three point moving average (with the weights: 1/4, 1/2, 1/4) was used. If one adjacent data point was not available, a two point moving average was used with the weights (1/3, 2/3) or (2/3, 1/3) if the right or left point, respectively, was missing. The range weights were symbolized by W_R in (4.1).

Smoothing was necessary because the cubic spline interpolation routines ICSEVU and IQHSCU (IMSL, 1984) would not work accurately with the spacially aliased raw data. Interpolation was required because GAME assumes that eigenray energy-flux densities are known at specified grazing angles.

Additional justification for smoothing comes from considering the random focusing and defocusing caused by lateral irregularities in the ocean bottom (Tuteur, 1976). Another reason is the effect on received energy of lateral variations in bottom structure (White, 1979). Smoothing over nearby grazing angles can also be justified (especially for higher order arrivals) because the sloping ocean bottom and horizontal ocean surface result in each bottom interaction having a different grazing angle (Itzikowitz et al., 1983). While the ocean bottom response may vary unpredictably, the source-receiver directionalities are assumed to be slowly varying, so they are

approximately constant for the three points averaged here. Thus, smoothing should correct for some lateral reflectivity smearing, while leaving source and receiver directionality information intact.

B.12 Determine grazing angles and interpolate energy-flux densities between measured grazing angles.

The BRL computation algorithm used in this study requires that energy-flux densities be available at constant values of grazing angle. However, data were not recorded at constant grazing angles. To obtain values at constant grazing angles the interpolation routines ICSEVU and IQHSCU were used (IMSL, 1984). The spatial density of the data required that one to four values be interpolated between data points.

B.13 Take ratios to compute BRL.

Using GAME to solve (2.1) is equivalent to treating the n data values as n equations in the two unknowns, BRL and BTL. We can solve for n-1 estimates of BRL. The bottom reflection loss estimates (in dB units) obtained by the algorithm are illustrated by (2.2). When (2.4) for a frequency band, Δf, is substituted into (2.2) the result is

$$BRL(\Delta f,g,N) = \{ [[N-1]BRL + BTL] - [[M-1]BRL + BTL] \} / [N-M] + e(N,M). \quad (B.4)$$

Here M, BRL, BTL and e are all functions of the frequency band and grazing angle. The term, e(N,M) (in dB), has been stated explicitly to recognize the presence of errors and unspecified losses in the eigenrays (they are discussed at the end of Section 2.2). The other factors are defined in Section 2.2. The n-1 BRL estimates are averaged to yield a final value. The error term, e, is reduced in the average, assuming the statistics given in Section 2.2. (The set of equations (B.4) could be solved in other ways. For example, the error, e, could be minimized in a least squares sense.)

B.14 Solve equations for BTL.

Instead of solving (2.4) for BRL, the loss BTL can be obtained. BTL can be expressed in a fashion similar to (2.2):

$$BTL(\Delta f,g) = -10\log_{10}\{ [E_m(\Delta f,g,N) / Spr_a(g,N)]^{[M(\Delta f,g)-1]} / [E_m(\Delta f,g,M) / Spr_a(g,M)]^{[N-1]} \} / [N-M(\Delta f,g)], \quad (B.5)$$

where $1 < M < N$ (or M=1 and N=2, in which case only the first eigenray was used). Equation 4.1 was used to compute the values E_m used here, with the quantity SUM in the frequency weights (B.2) set equal to the sum of the frequency taper function values. The other factors were identified in Section 2.2.

After the source function is cancelled and spreading and surface decoupling loss corrections are applied, the result (similar to

Equation B.4) is:

$$BTL(\Delta f,g,N) = \{ [M-1][[N-1]BRL + BTL] - [N-1][[M-1]BRL + BTL] \} / [N-M] + e(N,M). \quad (B.6)$$

Here M, BRL, BTL and e are all functions of both frequency band and grazing angle. The error term, e, fulfills the same purpose as it did in Appendix B.13 above. Again, a set of equations (B.6) could be solved by minimizing the error term, e, in a least squares sense.

In the BTL computation any errors in the eigenray energy-flux densities are magnified, compared to the BRL computation, because of the exponentiations by (M-1) and (N-1) in Equation B.5. In addition, errors which preferentially affect the eigenray with fewer bounces (E(M)) are increased relative to errors which preferentially affect E(N) or errors which affect both equally. This is because E(M) is raised to a higher number (N-1). These errors will appear in the term, e, of Equation B.6. (Again as in Appendix B.13 above, the error term is reduced when the BTL estimates are averaged, assuming the statistics given in Section 2.2.)

B.15 Compute the weighted average of BRL or BTL.

A weighted average of the individual BRL and BTL estimates was computed yielding an average value for each grazing angle and frequency band (4.2). The weight for each data signal, W_{SN}, is defined in terms of the measured, noise-contaminated energy-flux density of the data,

$E_{m,noisydata}$, and the measured energy-flux density of the noise alone, $E_{m,noise}$, as follows:

$$W_{SN}(f,r) = 10\log_{10} \left\{ [\, E_{m,noisydata}(f,r) \,] \,/\, E_{m,noise}(f,r) \right\} / \text{SUM},$$

where

$$\text{SUM} = \sum_{j=1}^{nf} 10\log_{10} \left\{ [\, E_{m,noisydata}(f_j,r) \,] \,/\, E_{m,noise}(f_j,r) \right\}$$

and "nf" is the number of discrete frequencies in the band being studied. This weighting function is a measure of the signal's visibility above the ambient noise. Ratios were computed for both the reference and reflected rays; the mean of these two ratios was used to weight the BRL and BTL estimates.